SIAM J. APPL. MATH.
Vol. 84, No. 3, pp. 961–987

FLOQUET STABILITY OF PERIODICALLY STATIONARY PULSES IN A SHORT-PULSE FIBER LASER*

VRUSHALY SHINGLOT† AND JOHN ZWECK†

Abstract. The quantitative modeling and design of modern short-pulse fiber lasers cannot be performed with averaged models because of large variations in the pulse parameters within each round trip. Instead, lumped models obtained by concatenating models for the various components of the laser are required. Since the optical pulses in lumped models are periodic, their linear stability is investigated using the monodromy operator, which is the linearization of the roundtrip operator about the pulse. A gradient-based optimization method is developed to discover periodic pulses. The computation of the gradient of the objective function involves numerical computation of the action of both the roundtrip operator and the adjoint of the monodromy operator. A novel Fourier split-step method is introduced to compute solutions of the linearization of the nonlinear, nonlocal, stiff equation that models optical propagation in the fiber amplifier. This method is derived by linearizing the two solution operators in a split-step method for the nonlinear equation. The spectrum of the monodromy operator consists of the essential spectrum, for which there is an analytical formula, and the eigenvalues. There is a multiplicity two eigenvalue at $\lambda = 1$, which is due to phase and translation invariance. The remaining eigenvalues are determined from a matrix discretization of the monodromy operator. Simulation results verify the accuracy of the numerical methods; show examples of periodically stationary pulses, their spectra, and their eigenfunctions; and discuss their stability.

Key words. fiber lasers, Floquet stability analysis, monodromy operator, nonlinear optics, split-step methods

MSC codes. 35B10, 35Q56, 37L15, 47D06, 78A60

DOI. 10.1137/23M1598106

1. Introduction.

Since the advent of the soliton laser [31], researchers have invented several generations of short-pulse fiber lasers, including dispersion-managed lasers [23, 42], similariton lasers [9, 13], and the Mamyshev oscillator [36, 40, 43]. The pulses in these lasers typically have durations on the order of 100 fs, peak powers on the order of 1 MW, and energy in the range of 1–50 nJ. Applications of femtosecond laser technology include frequency comb generation; highly accurate measurement of time, frequency, and distance; optical waveform generation; and laser surgery [8, 11].

Traditionally, the modeling of short-pulse lasers has been based on averaged models, in which each of the physical effects that act on the light pulse is averaged over one round trip of the laser loop to obtain a constant coefficient PDE, such as the cubic-quintic complex Ginzburg–Landau equation or the Haus master equation (HME) (see [24] for a review). This approach has been successfully applied to soliton lasers for which the pulse maintains its shape as it propagates. However, as is highlighted by Turitsyn, Bale, and Fedoruk [45], averaged models cannot be used for the quantitative modeling and design of recent generations of short-pulse lasers due to large variations in the pulse within each round trip.

Instead, the computational modeling of modern short-pulse lasers should be based on lumped models obtained by concatenating models for the various components of

*Received by the editors September 7, 2023; accepted for publication (in revised form) February 15, 2024; published electronically May 10, 2024.
https://doi.org/10.1137/23M1598106
Funding: This work was funded by the NSF under DMS-2106203.

†Department of Mathematical Sciences, The University of Texas at Dallas, Richardson, TX 75080 USA (vrushaly92296@gmail.com, zweck@utdallas.edu).

the laser. Typically, short-pulse lasers include an optical fiber amplifier, segments of single-mode fiber, a saturable absorber, a dispersion compensating element, a spectral filter, and an output coupler. With a lumped model, the pulse changes shape as it propagates through the various components of the laser system, returning to the same shape once per round trip. We call such pulses periodically stationary to distinguish them from the stationary pulses in a soliton laser.

Building on work of Kaup [21] and Haus [14, 15], Menyuk and Wang [30] developed a computational approach to the modeling of stationary pulse solutions of averaged models. With this method, stationary pulses are found using a root finding method, and their linear stability is determined by computing the spectrum of the linearization of the governing equation about the pulse. While there is an analytical formula for the essential spectrum, the eigenvalues must be numerically computed either by solving a (possibly nonlinear) eigenproblem involving a matrix discretization of the differential operator [37, 48] or by using Evans function methods [6, 17, 18, 19, 20].

In this paper, we extend this approach to periodically stationary pulses in lumped laser models. To keep the presentation concrete, we focus on a dispersion-managed laser of Kim et al. [23]. However, the methodology can readily be adapted to other lumped laser models. First, in section 2, we describe our lumped model of the Kim laser. The single-mode fiber segments are modeled by the nonlinear Schrödinger equation (NLSE), and the fiber amplifier is modeled by the HME, which is a generalization of the NLSE that includes a nonlocal saturable gain term. We also introduce the roundtrip operator $\mathcal{R}$, which models propagation once around the laser loop, and define a pulse, ψ, to be periodically stationary if $\mathcal{R}\psi = e^{i\theta}\psi$ for some constant phase θ. In section 3, we introduce the monodromy operator $\mathcal{M}$, which is the linearization of $\mathcal{R}$ about a pulse, ψ. We formulate the equations for the linearization of each component of the model, focusing special attention on the linearization of the HME. Because the nonlinear PDEs in the model involve the complex conjugate of ψ, we choose to define $\mathcal{M}$ to act on $\mathbb{R}^2$-valued functions, which should be thought of as the real and imaginary parts of $\mathbb{C}$-valued functions.

In section 4, we develop a computational method for discovering periodically stationary pulses. This method, which involves using gradient-based optimization to minimize the L^2-error between $\mathcal{R}\psi$ and $e^{i\theta}\psi$, is an adaptation of a method of Ambrose and Wilkening for computing periodic solutions of PDEs [2]. In particular, we provide an analytical formula for the optimal phase θ in terms of the optimal pulse ψ. The computation of the gradient of the objective function involves numerical computation of the action of both the roundtrip operator $\mathcal{R}$ and the adjoint $\mathcal{M}^*$ of the monodromy operator.

In section 5, we describe the Fourier split-step methods we use to solve the HME and its linearization. For the HME, we use a method of Wang et al. [47] designed to handle the frequency filtering term in the equation, which is nonlinear, nonlocal, and stiff. In particular, we provide formulae for locally third-order-accurate solution operators for the two steps in the method. Then we derive the split-step method for the linearized equation by linearizing these two solution operators. To the best of our knowledge, this approach is novel even in the special case of the linearized NLSE. Finally, the solver for the linearization is then used to obtain one for its adjoint. The derivation of these methods is not completely straightforward due to the nonlocal nature of the saturable gain term in the HME.

In analogy with the Floquet theory of periodic solutions of ODEs [44], we expect that the linear stability of a periodically stationary pulse will be determined by the spectrum of the monodromy operator. The spectrum of $\mathcal{M}$ is the union of the essential

spectrum and the eigenvalues. In [38], we derived a formula for the essential spectrum. In section 6, we show that the monodromy operator has a multiplicity two eigenvalue at $\lambda = 1$, which is due to the phase and time translation invariances of $\mathcal{R}$. These eigenvalues are analogous to the well-known eigenvalues of stationary pulses at $\lambda = 0$ [21]. As in [7, 39], we determine the remaining eigenvalues from a matrix discretization of $\mathcal{M}$. Finally, in section 7, we present simulation results that verify the accuracy of the numerical methods; show examples of periodically stationary pulses, their spectra, and their eigenfunctions; and discuss their stability.

Some of the results in this paper were announced in [38, 39]. However, the spectra shown here are for a new modified version of the monodromy operator introduced in section 6.

2. Mathematical model. In the left panel of Figure 1, we show a system diagram for the lumped model of the stretched pulse laser of Kim et al. [23]. A light pulse circulates around the loop, passing through a saturable absorber (SA), a segment of single-mode fiber (SMF1), a fiber amplifier (FA), a second segment of single-mode fiber (SMF2), a dispersion compensation element (DCF), and an output coupler (OC). After several round trips, the light circulating in the loop forms into a pulse that changes shape as it propagates through the different components, returning to the same shape each time it returns to the same position in the loop. In the right panel of Figure 1, we show the profile of such a periodically stationary pulse at the output of each component. The goal of this paper is to study the spectral stability of such periodically stationary pulses in lumped models of fiber lasers.

At each position in the loop, we model the complex electric field envelope of the light as a function, $\psi = \psi(x)$. Physically speaking, x is a fast-time variable defined relative to a frame moving at the group velocity [30, 52]. Since the length of the optical fiber in the loop is on the order of 1 m and the loop contains a single pulse with duration on the order of 100 fs, the pulse duration is about one ten-thousandth of the roundtrip time. Consequently, it is reasonable to assume that the fast-time variable x varies over the entire real line $\mathbb{R}$ rather than being periodic. Of course, in numerical computations, we truncate $\mathbb{R}$ to a finite interval. The pulse is normalized so that $|\psi(x)|^2$ is the instantaneous power. We assume that the function ψ is an element of the Lebesgue space $L^2(\mathbb{R}, \mathbb{C})$ of square integrable, complex-valued functions on $\mathbb{R}$. We model each component of the laser as a transfer function, $\mathcal{P} : L^2(\mathbb{R}, \mathbb{C}) \to L^2(\mathbb{R}, \mathbb{C})$, so that

$$\psi_{\text{out}} = \mathcal{P}\psi_{\text{in}}, \tag{2.1}$$

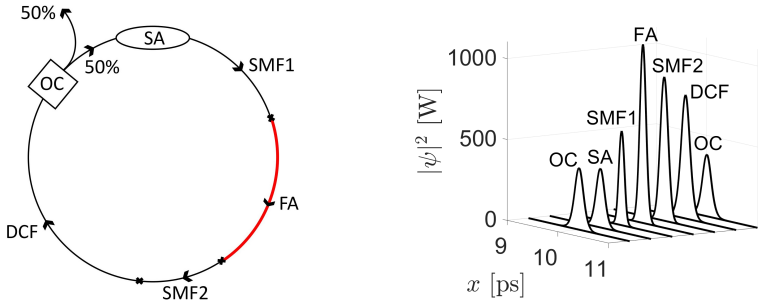

FIG. 1. *Left: System diagram of the stretched pulse laser of Kim et al.* [23]. *Right: Instantaneous power of the periodically stationary pulse exiting each component of the laser.*

where ψ_{in} and ψ_{out} are the pulses entering and exiting the component. The components in the model come in two flavors: discrete and continuous. By a discrete component, we mean one in which the action of the operator $\mathcal{P}$ on the input pulse ψ_{in} is essentially obtained in one step, for example, by the application of an explicit formula. In our model of the Kim laser, the discrete components are the saturable absorber, dispersion compensation element, and output coupler. Short-pulse fiber lasers sometimes also include a spectral filter that is modeled as a discrete component. By a continuous component, we mean one in which the action of the operator $\mathcal{P}$ on the input pulse ψ_{in} is modeled by solving a nonlinear wave equation with initial condition ψ_{in} from the input to the output of the component. In fiber lasers, the continuous components are those that involve the propagation of a light pulse through a segment of nonlinear optical fiber. For our model of the Kim laser, these are the fiber amplifier and the two segments of single-mode fiber. Note that we have chosen to model the dispersion compensation element as a discrete component since it is modeled by a constant-coefficient linear PDE which has an analytical solution in the Fourier domain.

With a lumped model, the propagation of a light pulse once around the laser loop is modeled by the roundtrip operator $\mathcal{R}: L^2(\mathbb{R},\mathbb{C}) \to L^2(\mathbb{R},\mathbb{C})$, which is given by the composition of the transfer functions of all the components. For our model of the Kim laser, the roundtrip operator is given by

$$\mathcal{R} = \mathcal{P}^{\text{OC}} \circ \mathcal{P}^{\text{DCF}} \circ \mathcal{P}^{\text{SMF2}} \circ \mathcal{P}^{\text{FA}} \circ \mathcal{P}^{\text{SMF1}} \circ \mathcal{P}^{\text{SA}}. \tag{2.2}$$

We say that $\psi_0 \in L^2(\mathbb{R},\mathbb{C})$ is a *periodically stationary pulse* if

$$\mathcal{R}(\psi_0) = e^{i\theta}\psi_0 \tag{2.3}$$

for some constant phase $\theta \in [0, 2\pi)$. For the Kim laser, ψ_0 is the pulse at the input to the saturable absorber. For each component, we let ψ_{in} denote the pulse obtained by propagating the periodically stationary pulse ψ_0 from the input of the SA to the input of that component. For the continuous fiber components, we let ψ denote the pulse propagating through that fiber.

We now describe the model for the propagation of a light pulse, $\psi = \psi(t,x)$, through the fiber amplifier. Here t denotes position along the fiber with $0 \le t \le L_{\text{FA}}$, where L_{FA} is the length of the fiber amplifier. We note that t is a local evolution variable that is only defined within the fiber amplifier. Our model for propagation in the fiber amplifier is based on the Haus master equation [14], which is a generalization of the NLSE that includes gain that saturates at high energy and is of finite bandwidth. Specifically, we model the transfer function $\mathcal{P}^{\text{FA}}$ of a fiber amplifier of length L_{FA} as $\psi_{\text{out}} = \mathcal{P}^{\text{FA}}\psi_{\text{in}}$, where $\psi_{\text{out}} = \psi(L_{\text{FA}}, \cdot)$ is obtained by solving the initial value problem

$$\begin{aligned} &\partial_t \psi = \left[\frac{g(\psi)}{2}\left(1 + \frac{1}{\Omega_g^2}\partial_x^2\right) - \frac{i}{2}\beta_{\text{FA}}\partial_x^2 + i\gamma|\psi|^2\right]\psi \qquad \text{for } 0 \le t \le L_{\text{FA}}, \\ &\psi(0,\cdot) = \psi_{\text{in}}. \end{aligned} \tag{2.4}$$

Here $g(\psi)$ is the saturable gain given by

$$g(\psi) = \frac{g_0}{1 + E(\psi)/E_{\text{sat}}}, \tag{2.5}$$

where g_0 is the unsaturated gain, E_{sat} is the saturation energy, and $E(\psi)$ is the pulse energy, which is given by

$$E(\psi) = \int_{\mathbb{R}} |\psi(\cdot,x)|^2 dx. \tag{2.6}$$

The saturable gain is modeled as a nonlocal function of the fast-time variable x since the response time of the fiber amplifier is on the order of 1 ms [32], which is much longer than the pulse duration, which is on the order of 100 fs. We also observe that the energy and saturable gain depend on the evolution variable t since ψ does. The finite bandwidth of the amplifier is modeled using a Gaussian filter with bandwidth Ω_g. In (2.4), β_{FA} is the chromatic dispersion coefficient, and γ is the nonlinear Kerr coefficient.

Similarly, we model the transfer function $\mathcal{P}^{\mathrm{SMF}}$ of a segment of single-mode fiber of length L_{SMF} as $\psi_{\mathrm{out}} = \mathcal{P}^{\mathrm{SMF}}\psi_{\mathrm{in}}$, where $\psi_{\mathrm{out}} = \psi(L_{\mathrm{SMF}}, \cdot)$ is obtained by solving the initial value problem for the NLSE given by

$$\begin{aligned} \partial_t \psi &= -\frac{i}{2}\beta_{\mathrm{SMF}}\partial_x^2\psi + i\gamma|\psi|^2\psi \qquad \text{for } 0 \le t \le L_{\mathrm{SMF}}, \\ \psi(0,\cdot) &= \psi_{\mathrm{in}}. \end{aligned} \tag{2.7}$$

We model the dispersion compensation element as $\mathcal{P}_{\mathrm{DCF}} = \mathcal{F}^{-1} \circ \widehat{\mathcal{P}}^{\mathrm{DCF}} \circ \mathcal{F}$, where $\mathcal{F}$ is the Fourier transform and

$$\widehat{\psi}_{\mathrm{out}}(\omega) = (\widehat{\mathcal{P}}^{\mathrm{DCF}}\widehat{\psi}_{\mathrm{in}})(\omega) = \exp\left(i\omega^2\beta_{\mathrm{DCF}}/2\right)\widehat{\psi}_{\mathrm{in}}(\omega) \tag{2.8}$$

with $\widehat{\psi} = \mathcal{F}(\psi)$. We observe that (2.8) is the solution to the initial value problem for the linear equation obtained by setting $\gamma = 0$, $\beta_{\mathrm{SMF}} = \beta_{\mathrm{DCF}}$, and $L_{\mathrm{SMF}} = 1$ in (2.7).

We model the saturable absorber using the fast saturable loss transfer function [49] $\mathcal{P}^{\mathrm{SA}}$ given by

$$\psi_{\mathrm{out}} = \mathcal{P}^{\mathrm{SA}}(\psi_{\mathrm{in}}) = \left(1 - \frac{\ell_0}{1 + |\psi_{\mathrm{in}}|^2/P_{\mathrm{sat}}}\right)\psi_{\mathrm{in}}, \tag{2.9}$$

where ℓ_0 is the unsaturated loss and P_{sat} is the saturation power. With this model, ψ_{out} at x only depends on ψ_{in} at the same value of x. Finally, we model the transfer function $\mathcal{P}^{\mathrm{OC}}$ of the output coupler as

$$\psi_{\mathrm{out}} = \mathcal{P}^{\mathrm{OC}}\psi_{\mathrm{in}} = \ell_{\mathrm{OC}}\,\psi_{\mathrm{in}}, \tag{2.10}$$

where $(\ell_{\mathrm{OC}})^2$ is the power loss at the output coupler.

3. Linearization of the roundtrip operator. In this section, we derive formulae for the linearizations $\mathcal{U}$ about a pulse of each of the operators $\mathcal{P}$ defined in section 2. By the chain rule, the linearization $\mathcal{M}$ of the roundtrip operator $\mathcal{R}$ about a periodically stationary pulse ψ_0 is equal to the composition of the linearized transfer functions $\mathcal{U}$ of each component of the system, i.e.,

$$\mathcal{M} = \mathcal{U}^{\mathrm{OC}} \circ \mathcal{U}^{\mathrm{DCF}} \circ \mathcal{U}^{\mathrm{SMF2}} \circ \mathcal{U}^{\mathrm{FA}} \circ \mathcal{U}^{\mathrm{SMF1}} \circ \mathcal{U}^{\mathrm{SA}}. \tag{3.1}$$

In analogy with the monodromy matrix in the Floquet theory of periodic solutions of ODEs [44], we call $\mathcal{M}$ the *monodromy operator* of the linearization of the roundtrip operator $\mathcal{R}$ about the periodically stationary pulse ψ_0. In [38], we provide conditions on the smoothness and decay of the pulse which ensure that the monodromy operator exists on an appropriate Lebesgue function space.

Because the linearization of the PDEs in the model involves the complex conjugate of ψ, we reformulate the model as a system of equations for the column vector $\boldsymbol{\psi} = [\mathrm{Re}(\psi), \mathrm{Im}(\psi)]^T \in \mathbb{R}^2$. For example, the transfer function of the fiber amplifier is

reformulated as the operator $\mathcal{P}^{\mathrm{FA}} : L^2(\mathbb{R},\mathbb{R}^2) \to L^2(\mathbb{R},\mathbb{R}^2)$ given by $\boldsymbol{\psi}_{\mathrm{out}} = \mathcal{P}^{\mathrm{FA}}\boldsymbol{\psi}_{\mathrm{in}}$, where $\boldsymbol{\psi}_{\mathrm{out}} = \boldsymbol{\psi}(\mathrm{L}_{\mathrm{FA}},\cdot)$ is obtained by solving the initial value problem

$$\begin{aligned} \partial_t \boldsymbol{\psi} &= \left[\frac{g(\boldsymbol{\psi})}{2}\left(1+\frac{1}{\Omega_g^2}\partial_x^2\right) - \frac{\beta}{2}\mathbf{J}\partial_x^2 + \gamma\left\|\boldsymbol{\psi}\right\|^2\mathbf{J}\right]\boldsymbol{\psi}, \\ \boldsymbol{\psi}(0,\cdot) &= \boldsymbol{\psi}_{\mathrm{in}}, \end{aligned} \tag{3.2}$$

where $\mathbf{J} = \left[\begin{smallmatrix} 0 & -1 \\ 1 & 0 \end{smallmatrix}\right]$ and $\|\cdot\|$ is the standard Euclidean norm on $\mathbb{R}^2$.

The linearized transfer function $\mathcal{U}^{\mathrm{FA}} : L^2(\mathbb{R},\mathbb{R}^2) \to L^2(\mathbb{R},\mathbb{R}^2)$ in the fiber amplifier is given by $\boldsymbol{u}_{\mathrm{out}} = \mathcal{U}^{\mathrm{FA}}\boldsymbol{u}_{\mathrm{in}}$, where $\boldsymbol{u}_{\mathrm{out}} = \boldsymbol{u}(L_{\mathrm{FA}},\cdot)$ is obtained by solving the linearized initial value problem

$$\begin{aligned} &\partial_t \boldsymbol{u} = \mathcal{L}^{\mathrm{FA}}(\boldsymbol{\psi})(\mathbf{u}) = \left[g(\boldsymbol{\psi})\mathcal{K} + \mathcal{L} + \mathcal{M}_1(\boldsymbol{\psi}) + \mathcal{M}_2(\boldsymbol{\psi}) + \mathcal{P}(\boldsymbol{\psi})\right]\boldsymbol{u}, \text{ for } 0 \le t \le L_{\mathrm{FA}}, \\ &\boldsymbol{u}(0,\cdot) = \boldsymbol{u}_{\mathrm{in}}, \end{aligned} \tag{3.3}$$

where

$$\begin{aligned} \mathcal{K} &= \frac{1}{2}\left(1+\frac{1}{\Omega_g^2}\partial_x^2\right), & \mathcal{L} &= -\frac{\beta}{2}\mathbf{J}\partial_x^2, \\ \mathcal{M}_1(\boldsymbol{\psi}) &= \gamma\left\|\boldsymbol{\psi}\right\|^2\mathbf{J}, & \mathcal{M}_2(\boldsymbol{\psi}) &= 2\gamma\mathbf{J}\boldsymbol{\psi}\boldsymbol{\psi}^T \end{aligned} \tag{3.4}$$

and

$$\mathcal{P}(\boldsymbol{\psi})\boldsymbol{u} = -\frac{g^2(\boldsymbol{\psi})}{g_0 E_{\mathrm{sat}}}\left[\left(1+\frac{1}{\Omega_g^2}\partial_x^2\right)\boldsymbol{\psi}\right]\int_{-\infty}^{\infty}\boldsymbol{\psi}^T(x)\boldsymbol{u}(x)dx \tag{3.5}$$

is a nonlocal operator. The nonlocality of $\mathbf{P}$, which arises because the gain saturation depends on the total energy of the pulse, makes the analysis more challenging for the fiber amplifier than for a segment of single-mode fiber. The linearized transfer function $\mathcal{U}^{\mathrm{SMF}}$ of a segment of single-mode fiber is obtained by setting $g(\boldsymbol{\psi}) = 0$ in (3.3) and (3.5).

The linearized transfer function $\mathcal{U}^{\mathrm{SA}}$ for the saturable absorber is given by

$$\boldsymbol{u}_{\mathrm{out}} = \mathcal{U}^{\mathrm{SA}}(\boldsymbol{\psi}_{\mathrm{in}})\boldsymbol{u}_{\mathrm{in}} = \left(1 - \ell(\boldsymbol{\psi}_{\mathrm{in}}) - \frac{2\ell^2(\boldsymbol{\psi}_{\mathrm{in}})}{\ell_0 P_{\mathrm{sat}}}\boldsymbol{\psi}_{\mathrm{in}}\boldsymbol{\psi}_{\mathrm{in}}^T\right)\boldsymbol{u}_{\mathrm{in}}, \tag{3.6}$$

where

$$\ell(\boldsymbol{\psi}_{\mathrm{in}}) = \frac{\ell_0}{1 + \left\|\boldsymbol{\psi}_{\mathrm{in}}\right\|^2/P_{\mathrm{sat}}}. \tag{3.7}$$

The remaining components, i.e., dispersion compensation fiber and output coupler, already have linear transfer functions, and so $\mathcal{U}^{\mathrm{DCF}} = \mathcal{P}^{\mathrm{DCF}}$ and $\mathcal{U}^{\mathrm{OC}} = \mathcal{P}^{\mathrm{OC}}$.

Because eigenvalues and eigenfunctions can be complex valued, we extend the linearized system to act on complex-valued functions $\boldsymbol{u} \in L^2(\mathbb{R},\mathbb{C}^2)$, where

$$L^2(\mathbb{R},\mathbb{C}^2) = \{\boldsymbol{u} = \boldsymbol{v} + i\boldsymbol{w} \,:\, \boldsymbol{v},\boldsymbol{w} \in L^2(\mathbb{R},\mathbb{R}^2)\} \tag{3.8}$$

is the space of $\mathbb{C}^2$-valued functions on $\mathbb{R}$ with the standard Hermitian inner product. Let $\mathcal{T}$ be an operator that acts on $\mathbb{R}^2$-valued functions. We extend $\mathcal{T}$ to act on $\mathbb{C}^2$-valued functions by defining $\mathcal{T}\boldsymbol{u} = \mathcal{T}\boldsymbol{u}_1 + i\mathcal{T}\boldsymbol{u}_2$, where $\boldsymbol{u} = \boldsymbol{u}_1 + i\boldsymbol{u}_2$ with $\boldsymbol{u}_1, \boldsymbol{u}_2 \in L^2(\mathbb{R},\mathbb{R}^2)$. Note that the formulae above for the action of the differential operators and transfer functions on $\mathbb{C}^2$-valued functions $\boldsymbol{u}$ are the same as for their action on $\mathbb{R}^2$-valued functions since in both cases we only require $\boldsymbol{\psi}$ to be $\mathbb{R}^2$-valued. The only difference is our interpretation of the function spaces on which they act.

4. Computation of periodically stationary pulses. We formulate the problem of finding periodically stationary pulses as that of finding a zero of the Poincaré map functional $\mathcal{E} : L^2(\mathbb{R}, \mathbb{R}^2) \times [0, 2\pi) \to \mathbb{R}$ given by

$$\mathcal{E}(\boldsymbol{\psi}_0, \theta) = \frac{1}{2} \left\| \mathcal{R}(\boldsymbol{\psi}_0) - \mathbf{R}(\theta)\boldsymbol{\psi}_0 \right\|^2_{L^2(\mathbb{R},\mathbb{R}^2)}, \tag{4.1}$$

where $\mathbf{R}(\theta)$ is the rotation matrix on $\mathbb{R}^2$ that corresponds to the operator of multiplication by $e^{i\theta}$ on $\mathbb{C}$.[1]

Next, we describe the two-stage method we use to compute periodically stationary pulse solutions $\boldsymbol{\psi}_0$ of the laser system model in section 2. In the first (evolutionary) stage, we propagate a Gaussian pulse over sufficiently many round trips of the laser to obtain a good initial guess for the second (optimization) stage. In the optimization stage, we use a gradient-based method to minimize the objective function given by the ratio of the Poincaré map functional (4.1) and the pulse energy, (2.6),

$$\widetilde{\mathcal{E}}(\psi_0, \theta) = \frac{\mathcal{E}(\psi_0, \theta)}{E(\psi_0)}. \tag{4.2}$$

We note that if ψ_0 is a nonzero periodically stationary pulse, then there is a θ so that $\widetilde{\mathcal{E}}$ has a global minimum value of zero at (ψ_0, θ). Therefore, to find nontrivial periodically stationary pulses, it makes sense to use an optimization algorithm to drive $\widetilde{\mathcal{E}}$ to zero. In parameter continuation studies, the first stage can be omitted if the optimal pulse computed with the previous set of system parameters is a good enough initial guess for optimization with the current set of parameters.

In the following theorem, we adapt a method of Ambrose and Wilkening [2] for computing the gradient of $\mathcal{E}$ with respect to the pulse. With this method, the cost of computing a directional derivative of $\mathcal{E}$ is comparable to that of propagating a pulse and its linearization for one round trip of the laser.

THEOREM 4.1. *The variational derivative of $\mathcal{E}$ with respect to $\boldsymbol{\psi}_0$ is given by*

$$D_{\boldsymbol{\psi}_0}\mathcal{E}(\mathbf{u}_0) = \left\langle \frac{\delta \mathcal{E}}{\delta \boldsymbol{\psi}_0},\ \mathbf{u}_0 \right\rangle_{L^2(\mathbb{R},\mathbb{R}^2)}, \tag{4.3}$$

where

$$\frac{\delta \mathcal{E}}{\delta \boldsymbol{\psi}}(\boldsymbol{\psi}_0) = \mathcal{M}^*(\mathbf{v}_0) - \mathbf{R}(-\theta)\mathbf{v}_0, \tag{4.4}$$

where $\mathbf{v}_0 := \mathcal{R}(\boldsymbol{\psi}_0) - \mathbf{R}(\theta)\boldsymbol{\psi}_0$ is a measure of how far $\boldsymbol{\psi}_0$ is from being periodically stationary and the adjoint of $\mathcal{M}$ is given by

$$\mathcal{M}^* = \left(\mathcal{U}^{\mathrm{SA}}\right)^* \circ \left(\mathcal{U}^{\mathrm{SMF1}}\right)^* \circ \left(\mathcal{U}^{\mathrm{FA}}\right)^* \circ \left(\mathcal{U}^{\mathrm{SMF2}}\right)^* \circ \left(\mathcal{U}^{\mathrm{DCF}}\right)^* \circ \left(\mathcal{U}^{\mathrm{OC}}\right)^*, \tag{4.5}$$

where, for each component, $\mathcal{U}^*$ is the adjoint of the corresponding operator $\mathcal{U}$.

In a fiber segment of length L, the adjoint of the linearized solution operator $\mathcal{U}$ for the fiber is given by

$$\mathbf{v}_L = \mathcal{U}^*\mathbf{v}_0 \tag{4.6}$$

[1] We note that for a given set of system parameters, there is no guarantee that a periodically stationary pulse exists.

with $\mathbf{v}_L = \mathbf{v}(L,\cdot)$. *Here* $\mathbf{v} = \mathbf{v}(s,\cdot)$ *is obtained by solving the adjoint linearized initial value problem given by*

$$\begin{aligned} \partial_s \mathbf{v}(s,\cdot) &= \mathcal{L}^*(\boldsymbol{\psi}(L-s,\cdot))\mathbf{v}(s,\cdot), \\ \mathbf{v}(0,\cdot) &= \mathbf{v}_0, \end{aligned} \tag{4.7}$$

where $\mathcal{L}^*(\boldsymbol{\psi})$ *is the adjoint of the linearized differential operator* $\mathcal{L}(\boldsymbol{\psi})$, *as in* (3.3).

Remark. Note that here we have $s = L - t$ so that solving the adjoint equation from $s = 0$ to $s = L$ propagates the initial pulse $\mathbf{v}_0$ backward in t from $t = L$ to $t = 0$. The formula for the operator $\mathcal{L}^*$ in a fiber segment is obtained from the formula for $\mathcal{L}$ in (3.3) by taking the transposes of all matrices. The operator $\mathcal{U}^{\mathrm{SA}}$ is self-adjoint.

Proof. The variational derivative of $\mathcal{E}$ with respect to $\boldsymbol{\psi}_0$ is given by

$$D_{\boldsymbol{\psi}_0}\mathcal{E}(\mathbf{u}_0) = \lim_{\epsilon\to 0}\frac{1}{\epsilon}\left(\mathcal{E}(\boldsymbol{\psi}_0 + \epsilon\mathbf{u}_0,\theta) - \mathcal{E}(\boldsymbol{\psi}_0,\theta)\right) \tag{4.8}$$

$$= \langle \mathcal{R}(\boldsymbol{\psi}_0) - \mathbf{R}(\theta)\boldsymbol{\psi}_0, \mathcal{M}(\mathbf{u}_0) - \mathbf{R}(\theta)\mathbf{u}_0\rangle_{L^2(\mathbb{R},\mathbb{R}^2)}, \tag{4.9}$$

where we have used the fact that $\mathcal{R}(\psi_0 + \epsilon u_0) \approx \mathcal{R}(\psi_0) + \epsilon\mathcal{M}(u_0)$. Setting $\mathbf{v}_0 := \mathcal{R}(\boldsymbol{\psi}_0) - \mathbf{R}(\theta)\boldsymbol{\psi}_0$, we find that

$$D_{\boldsymbol{\psi}_0}\mathcal{E}(\mathbf{u}_0) = \langle \mathcal{M}^*(\mathbf{v}_0) - \mathbf{R}(-\theta)\mathbf{v}_0, \mathbf{u}_0\rangle_{L^2(\mathbb{R},\mathbb{R}^2)}, \tag{4.10}$$

which proves (4.3).

To derive (4.7), we invoke the defining formula for $\mathcal{U}^*$:

$$\langle \mathbf{v}_0, \mathbf{u}_L\rangle = \langle \mathbf{v}_0, \mathcal{U}(\mathbf{u}_0)\rangle = \langle \mathcal{U}^*(\mathbf{v}_0), \mathbf{u}_0\rangle = \langle \mathbf{v}_L, \mathbf{u}_0\rangle. \tag{4.11}$$

Next, we set $s = L - t$ and introduce a function $\mathbf{v} = \mathbf{v}(s,x)$ to be chosen so that

$$h(s) = \langle \mathbf{v}(s,\cdot),\ \mathbf{u}(L-s,\cdot)\rangle_{L^2(\mathbb{R},\mathbb{R}^2)} \tag{4.12}$$

is constant. Then $\mathbf{v}_L = \mathbf{v}(L,\cdot)$ will satisfy (4.11) as required. To derive an equation for $\mathbf{v}$, we differentiate h to obtain

$$\begin{aligned} h'(s) &= \langle \partial_s\mathbf{v}(s,\cdot),\ \mathbf{u}(L-s,\cdot)\rangle_{L^2(\mathbb{R},\mathbb{R}^2)} - \langle \mathbf{v}(s,\cdot),\ \partial_t u(L-s,\cdot)\rangle_{L^2(\mathbb{R},\mathbb{R}^2)} \\ &= \langle \partial_s\mathbf{v}(s,\cdot),\ \mathbf{u}(L-s,\cdot)\rangle_{L^2(\mathbb{R},\mathbb{R}^2)} - \langle \mathbf{v}(s,\cdot),\ \mathcal{L}(\boldsymbol{\psi}(L-s,\cdot))\mathbf{u}(L-s,\cdot)\rangle_{L^2(\mathbb{R},\mathbb{R}^2)} \\ &= \langle \partial_s\mathbf{v}(s,\cdot) - \mathcal{L}^*(\boldsymbol{\psi}(L-s,\cdot))\mathbf{v}(s,\cdot),\ \mathbf{u}(L-s,\cdot)\rangle_{L^2(\mathbb{R},\mathbb{R}^2)}, \end{aligned}$$

which is zero provided that $\mathbf{v}$ satisfies the initial value problem (4.7). ∎

Next, we derive an analytical formula for the derivative of $\mathcal{E}$ with respect to θ. For this result, it is easier to work over $\mathbb{C}$ than $\mathbb{R}^2$.

Proposition 4.2. *Suppose that* (ψ_0,θ) *is a local minimum of*

$$\mathcal{E}(\psi_0,\theta) = \frac{1}{2}\|\mathcal{R}(\psi_0) - e^{i\theta}\psi_0\|_{L^2(\mathbb{R},\mathbb{C})}. \tag{4.13}$$

Then $\theta = \theta(\psi_0)$ *is given in terms of* ψ_0 *by*

$$(\cos\theta, \sin\theta) = \frac{1}{\sqrt{G^2(\psi_0) + H^2(\psi_0)}}(G(\psi_0), H(\psi_0)), \tag{4.14}$$

where

$$F(\psi_0) = \frac{1}{2}\left\{\|\mathcal{R}(\psi_0)\|^2_{L^2(\mathbb{R},\mathbb{C})} + \|\psi_0\|^2_{L^2(\mathbb{R},\mathbb{C})}\right\},$$
$$G(\psi_0) = \mathrm{Re}\langle \mathcal{R}(\psi_0), \psi_0\rangle, \quad H(\psi_0) = \mathrm{Im}\langle \mathcal{R}(\psi_0), \psi_0\rangle. \tag{4.15}$$

Let

$$\mathcal{F}(\psi_0) := \mathcal{E}(\psi_0, \theta(\psi_0)) = F(\psi_0) - \sqrt{G^2(\psi_0) + H^2(\psi_0)}. \tag{4.16}$$

Then

$$\frac{\delta \mathcal{F}}{\delta \psi}(\psi_0) = \frac{\delta \mathcal{E}}{\delta \psi}(\psi_0, \theta(\psi_0)), \tag{4.17}$$

where $\frac{\delta \mathcal{E}}{\delta \psi}(\psi_0, \theta(\psi_0))$ *is given by* (4.4). *Furthermore,* (ψ_0, θ) *is a local minimum of* $\mathcal{E}$ *iff* ψ_0 *is a local minimum of* $\mathcal{F}$.

Proof. By (4.13),

$$\begin{aligned}\mathcal{E}(\psi_0, \theta) &= \frac{1}{2}\left\{\|\mathcal{R}(\psi_0)\|^2_{L^2(\mathbb{R},\mathbb{C})} + \|\psi_0\|^2_{L^2(\mathbb{R},\mathbb{C})}\right\} - \mathrm{Re}\langle e^{-i\theta}\mathcal{R}(\psi_0), \psi_0\rangle_{L^2(\mathbb{R},\mathbb{C})} \\ &= F(\psi_0) - \left(G(\psi_0)\cos\theta + H(\psi_0)\sin\theta\right). \end{aligned} \tag{4.18}$$

Therefore, $\frac{\partial \mathcal{E}}{\partial \theta} = 0$ iff

$$(\cos\theta, \sin\theta) = \frac{\pm 1}{\sqrt{G^2(\psi_0) + H^2(\psi_0)}}(G(\psi_0), H(\psi_0)). \tag{4.19}$$

To determine which of the signs in (4.19) corresponds to a local minimum of $\mathcal{E}(\theta)$, we observe that when θ satisfies (4.19), the second derivative of $\mathcal{E}$ is given by

$$\frac{\partial^2 \mathcal{E}}{\partial \theta^2} = G(\psi_0)\cos\theta + H(\psi_0)\sin\theta = \pm\sqrt{G^2(\psi_0) + H^2(\psi_0)}. \tag{4.20}$$

Substituting the value of θ given by (4.19) with the + sign into (4.18), we obtain (4.16). Finally, since

$$\frac{\delta \mathcal{F}}{\delta \psi}(\psi_0) = \frac{\delta \mathcal{E}}{\delta \psi}(\psi_0, \theta(\psi_0)) + \frac{\delta \mathcal{E}}{\delta \theta}(\psi_0, \theta(\psi_0))\frac{\delta \theta}{\delta \psi}(\psi_0) \tag{4.21}$$

and $\frac{\delta \mathcal{E}}{\delta \theta}(\psi_0, \theta(\psi_0)) = 0$, we obtain (4.17). ∎

5. Fourier split-step method. In this section, we describe the Fourier split-step schemes we use to solve for the nonlinear propagation of the pulse $\boldsymbol{\psi}$ and its linearization $\mathbf{u}$ in the fiber segments. These methods are based on the well-known symmetric split-step scheme for the NLSE, which is globally second-order accurate [50]. Wang et al. [47] show that, in addition to being nonlinear, the frequency filtering term $g(\boldsymbol{\psi})\boldsymbol{\psi}_{xx}$ in the fiber amplifier equation (2.4) is stiff. Therefore, we make use of a numerical method they designed to handle this stiff term. With this method, we propagate the pulse for one time step with the aid of a frequency domain solution operator for the stiff frequency filtering and chromatic dispersion terms and of a fast-time domain solution operator for the Kerr nonlinearity term. We then derive a split-step method for the linearized equation (3.3) by linearizing these two solution operators. This approach yields explicit locally third-order-accurate analytical formulae that do not involve the numerical computation of integrals over time. To the best of our knowledge, this approach is novel even in the special case of the linearized NLSE.

5.1. Operator splitting. The level of rigor in discussions of the symmetric split-step Fourier method for nonlinear wave equations varies widely [1, 3, 25, 33, 41, 50, 52]. At one end of the spectrum is the rigorous convergence result of Lubich [26]. At the other end are discussions that do not even explicitly address the sense in which the solution of $\partial_t \mathbf{f} = \mathcal{C}(t)\mathbf{f}$ is $\mathbf{f}(t) = \exp(\int_0^t \mathcal{C}(s)\,ds)\mathbf{f}(0)$. Here we are thinking of $\mathcal{C}(t)$ as being the differential operator on the right-hand side of the equation. Indeed, equality is not guaranteed to hold unless $\mathcal{C}(t_1)\mathcal{C}(t_2) = \mathcal{C}(t_2)\mathcal{C}(t_1)$ for all t_1, t_2, which is not even true in the case of the NLSE. To provide an accessible explanation as to why the symmetric split-step Fourier methods for the fiber amplifier equation (2.4) and its linearization (3.3) are locally third-order accurate, we begin with a discussion of operator splitting in this context.

PROPOSITION 5.1. *The solution to* $\partial_t \mathbf{f} = \mathcal{C}(t)\mathbf{f}$ *is of the form*

$$\mathbf{f}(t+h) = \exp\left(\int_t^{t+h} \mathcal{C}(s)\,ds\right)\mathbf{f}(t) \;+\; \mathcal{O}(h^3). \tag{5.1}$$

Proof. For simplicity, we assume $t = 0$. Substituting

$$\mathbf{f}(h) = \mathbf{f}_0 + h\mathbf{f}_1 + h^2\mathbf{f}_2 + \mathcal{O}(h^3), \tag{5.2}$$

$$\mathcal{C}(h) = \mathcal{C}_0 + h\mathcal{C}_1 + h^2\mathcal{C}_2 + \mathcal{O}(h^3) \tag{5.3}$$

into the differential equation and equating coefficients of h, we find that

$$\mathbf{f}(h) = \mathbf{f}_0 + h\mathcal{C}_0\mathbf{f}_0 + \frac{1}{2}h^2\left(\mathcal{C}_0^2\mathbf{f}_0 + \mathcal{C}_1\mathbf{f}_0\right) + \mathcal{O}(h^3) \tag{5.4}$$

$$= \left[\exp\left(\mathcal{C}_0 h\right) + \frac{1}{2}h^2\mathcal{C}_1\right]\mathbf{f}_0 + \mathcal{O}(h^3) \tag{5.5}$$

$$= \exp\left(\int_0^h \mathcal{C}(s)\,ds\right)\mathbf{f}_0 + \mathcal{O}(h^3). \tag{5.6}$$

∎

The nonlinear and linearized equations in the fiber amplifier are both of the form

$$\partial_t \mathbf{f} = (\mathcal{A}(t) + \mathcal{B}(t))\mathbf{f}, \tag{5.7}$$

where, for the nonlinear equation (with $\mathbf{f} = \boldsymbol{\psi}$),

$$\mathcal{A}(t) = \mathcal{L} + g(\boldsymbol{\psi}(t))\mathcal{K} \qquad \text{and} \qquad \mathcal{B}(t) = \mathcal{M}_1(\boldsymbol{\psi}(t)) \tag{5.8}$$

and, for the linear equation (with $\mathbf{f} = \mathbf{u}$),

$$\mathcal{A}(t) = \mathcal{L} + g(\boldsymbol{\psi}(t))\mathcal{K} + \mathcal{P}(\boldsymbol{\psi}(t)) \qquad \text{and} \qquad \mathcal{B}(t) = \mathcal{M}_1(\boldsymbol{\psi}(t)) + \mathcal{M}_2(\boldsymbol{\psi}(t)). \tag{5.9}$$

Let

$$\mathcal{A}_1(h) := \int_t^{t+h/2} \mathcal{A}(s)\,ds = \widetilde{\mathcal{A}}_1 h/2 \qquad \mathcal{A}_2(h) := \int_{t+h/2}^{t+h} \mathcal{A}(s)\,ds = \widetilde{\mathcal{A}}_2 h/2 \tag{5.10}$$

$$\mathcal{B}_0(h) := \int_t^{t+h} \mathcal{B}(s)\,ds = \widetilde{\mathcal{B}} h, \tag{5.11}$$

where the final equalities follow from the mean value theorem for integrals. In the special case of the NLSE, $\mathcal{A}(t) = \mathcal{A}$ is t-independent, and so the symmetric split-step scheme

$$\begin{aligned}\boldsymbol{\psi}(t+h) &= \exp\left(\mathcal{A}h + \mathcal{B}_0(h)\right)\boldsymbol{\psi}(t) + \mathcal{O}(h^3)\\ &= \exp\left(\mathcal{A}h/2\right)\exp\left(\mathcal{B}_0(h)\right)\exp\left(\mathcal{A}h/2\right)\boldsymbol{\psi}(t) + \mathcal{O}(h^3)\end{aligned} \tag{5.12}$$

holds by two applications of the Baker–Campbell–Haussdorff formula

$$\exp(\mathcal{X}h)\exp(\mathcal{Y}h) = \exp\left((\mathcal{X}+\mathcal{Y})\,h + \frac{1}{2}[\mathcal{X},\mathcal{Y}]h^2\right) + \mathcal{O}(h^3), \tag{5.13}$$

where $[\mathcal{X},\mathcal{Y}] = \mathcal{X}\mathcal{Y} - \mathcal{Y}\mathcal{X}$. We note, however, that for general operators $\widetilde{\mathcal{A}}_1$ and $\widetilde{\mathcal{A}}_2$,

$$\exp\left([\widetilde{\mathcal{A}}_2 + \widetilde{\mathcal{B}} + \widetilde{\mathcal{A}}_1]h\right) \neq \exp\left(\widetilde{\mathcal{A}}_2 h\right)\exp\left(\widetilde{\mathcal{B}}h\right)\exp\left(\widetilde{\mathcal{A}}_1 h\right) + \mathcal{O}(h^3). \tag{5.14}$$

Nevertheless, we will now show that equality holds in (5.14) for the operators in (5.10). Keeping only terms of order $< h^3$, we find that in general,

$$\exp(\mathcal{A}_2)\exp(\mathcal{B}_0)\exp(\mathcal{A}_1) = \exp\left(\mathcal{A}_1 + \mathcal{A}_2 + \mathcal{B}_0 + \frac{1}{2}[\mathcal{B}_0, \mathcal{A}_1 - \mathcal{A}_2] + [\mathcal{A}_2, \mathcal{A}_1]\right). \tag{5.15}$$

Therefore, it suffices to show that for the operators in (5.10), $\mathcal{A}_1 - \mathcal{A}_2 = \mathcal{O}(h^2)$ and $[\mathcal{A}_2, \mathcal{A}_1] = \mathcal{O}(h^3)$. Using Taylor series, these results follow from the formulae

$$\mathcal{A}_1(h) = \frac{h}{2}\left[\mathcal{A}(t) + \frac{h}{4}\mathcal{A}'(t)\right] + \mathcal{O}(h^3), \tag{5.16}$$

$$\mathcal{A}_2(h) = \frac{h}{2}\left[\mathcal{A}\left(t+\frac{h}{2}\right) + \frac{h}{4}\mathcal{A}'\left(t+\frac{h}{2}\right)\right] + \mathcal{O}(h^3), \tag{5.17}$$

$$\mathcal{A}_2(h) - \mathcal{A}_1(h) = \frac{h}{2}\left[\frac{h}{2}\mathcal{A}'(t) + \frac{h^2}{8}\mathcal{A}''(t)\right] + \mathcal{O}(h^3). \tag{5.18}$$

To summarize, the symmetric split-step scheme for (5.7) is given by

$$\mathbf{f}(t+h) = \exp(\mathcal{A}_2(h))\exp(\mathcal{B}_0(h))\exp(\mathcal{A}_1(h))\ \mathbf{f}(t) + \mathcal{O}(h^3). \tag{5.19}$$

For greater computational efficiency, we use Richardson extrapolation to combine solutions with step sizes of h, $h/2$, and $h/4$ to obtain the globally fourth-order-accurate scheme,

$$\mathbf{f}_k = \frac{1}{21}\left[32\mathbf{f}_k^{h/4} - 12\mathbf{f}_k^{h/2} + \mathbf{f}_k^{h}\right], \tag{5.20}$$

where $\mathbf{f}_k^h$ is the solution at time step k obtained using (5.19) with a step size of h.

5.2. Solution operators for the nonlinear equations. Next, we state two propositions that give analytical formulae for the two solution operators for the nonlinear equation (3.2) in the fiber amplifier. Setting $g = 0$ gives the corresponding results for the single-mode fiber segments.

PROPOSITION 5.2. *The solution operator for the Kerr nonlinearity term,*

$$\partial_t \boldsymbol{\psi} = \gamma \|\boldsymbol{\psi}\|^2 \mathbf{J}\,\boldsymbol{\psi}, \tag{5.21}$$

in the nonlinear equation (3.2) *for the fiber amplifier is given by*

$$\boldsymbol{\psi}(t+h,x) = \exp\left(\gamma \int_t^{t+h} \|\boldsymbol{\psi}(s,x)\|^2\,\mathbf{J}\,ds\right)\boldsymbol{\psi}(t,x) = \mathbf{R}(\gamma\|\boldsymbol{\psi}(t,x)\|^2 h)\boldsymbol{\psi}(t,x), \tag{5.22}$$

where

$$\mathbf{R}(b) = \begin{bmatrix} \cos b & -\sin b \\ \sin b & \cos b \end{bmatrix}. \tag{5.23}$$

Proof. Applying (5.21), we see that $\|\boldsymbol{\psi}(s,x)\|^2$ is constant in s. The result now follows from the fact that

$$\exp(a\mathbf{I}+b\mathbf{J}) = e^a\,\mathbf{R}(b). \tag{5.24}$$

∎

PROPOSITION 5.3. *The solution operator for the term*

$$\partial_t\boldsymbol{\psi} = (\mathcal{L}+g(\boldsymbol{\psi}(t,\cdot))\mathcal{K})\;\boldsymbol{\psi} \tag{5.25}$$

in the nonlinear equation (3.2) *for the fiber amplifier is given by*

$$\begin{aligned}\boldsymbol{\psi}(t+h/2,x) &= \exp\left(\int_t^{t+h/2}\mathcal{L}+g(\boldsymbol{\psi}(s,\cdot))\mathcal{K}\,ds\right)\boldsymbol{\psi}(t,x)\\ &= \mathcal{F}^{-1}\left(e^{G(t,t+h/2)a(\omega)}\,\mathbf{R}(b(\omega)h/2)\,\widehat{\boldsymbol{\psi}}(t,\omega)\right),\end{aligned} \tag{5.26}$$

where $\mathcal{F}$ is the Fourier transform,

$$a(\omega) = \frac{1}{2}\left(1-\frac{\omega^2}{\Omega_g^2}\right) \qquad \text{and} \qquad b(\omega) = \frac{1}{2}\beta\omega^2, \tag{5.27}$$

and

$$G(t,t+h/2) = \int_t^{t+h/2} g(\boldsymbol{\psi}(s))\,ds. \tag{5.28}$$

Finally, to compute $\boldsymbol{\psi}(t+h/2,\cdot)$ only in terms of $\boldsymbol{\psi}(t,\cdot)$, we employ the approximation

$$G(t,t+h/2) = \frac{h}{2}\left(g(t)+\frac{h}{4}g_2(t)\right)+\mathcal{O}(h^3), \tag{5.29}$$

where $g(t)=g(\boldsymbol{\psi}(t,\cdot))$ is given by (2.5) *and*

$$g_2(t) \;:=\; g'(t) = \frac{-2g^2(t)}{g_0E_{\rm sat}}\mathrm{Re}\int_{-\infty}^{\infty}[\widehat{\boldsymbol{\psi}}(t,\omega)]^*\,(b(\omega)\mathbf{J}+g(t)a(\omega)\mathbf{I})\,\widehat{\boldsymbol{\psi}}(t,\omega)\,d\omega, \tag{5.30}$$

where $\mathbf{v}^*$ denotes the conjugate transpose of a column vector $\mathbf{v}^*$.

Proof. Equation (5.26) follows from the fact that

$$\mathcal{L}+g(\boldsymbol{\psi}(s))\mathcal{K} = \mathcal{F}^{-1}\circ(b(\omega)h\,\mathbf{J}\;+\;G(t,t+h)a(\omega)\,\mathbf{I})\circ\mathcal{F} \tag{5.31}$$

and then applying (5.24). The derivation of (5.29) is the same as that of (5.16). Finally, (5.30) follows from (2.5), the formula

$$E'(t) = 2\mathrm{Re}\int_{-\infty}^{\infty}[\widehat{\boldsymbol{\psi}}(t,\omega)]^*\partial_t\widehat{\boldsymbol{\psi}}(t,\omega)\,d\omega \tag{5.32}$$

for the derivative of the pulse energy, and (5.25). ∎

Remark. In practice, it is enough to implement a split-step solver for the scalar field $\psi\in\mathbb{C}$ rather than the vector field $\boldsymbol{\psi}\in\mathbb{R}^2$ as was done in [47]. The reason for providing the solution operators, (5.22) and (5.26), in the vector case is that in the next subsection, we will use them to derive solution operators for the linearized equation. ∎

5.3. The linearized solution operators. Next, we state two propositions that give analytical formulae for the two solution operators for the linearized equation (3.3) in the fiber amplifier. Setting $g = 0$ gives the corresponding results for the single-mode fiber segments.

PROPOSITION 5.4. *The solution operator for the linearization*

$$\partial_t \mathbf{u} = [\mathcal{M}_1(\boldsymbol{\psi}) + \mathcal{M}_2(\boldsymbol{\psi})]\,\mathbf{u} \tag{5.33}$$

of the Kerr nonlinearity term in the linearized equation (3.3) *for the fiber amplifier is*

$$\begin{aligned}\mathbf{u}(t+h,x) &= \exp\left(\int_t^{t+h} [\mathcal{M}_1(\boldsymbol{\psi}(s)) + \mathcal{M}_2(\boldsymbol{\psi}(s))]\, ds\right)\mathbf{u}(t,x)\\ &= \mathbf{R}(\gamma\|\boldsymbol{\psi}(t,x)\|^2 h)\left(\mathbf{I} + 2\gamma h\,\mathbf{J}\boldsymbol{\psi}(t)\boldsymbol{\psi}(t)^T\right)\mathbf{u}(t,x).\end{aligned} \tag{5.34}$$

Proof. Suppose that $\mathbf{u}$ solves (5.33). Then $\boldsymbol{\psi}_\epsilon = \boldsymbol{\psi} + \epsilon\mathbf{u}$ solves (5.21), and so by Proposition 5.2,

$$\boldsymbol{\psi}_\epsilon(t+h) = F(\epsilon)\boldsymbol{\psi}_\epsilon(t), \quad \text{where } F(\epsilon) = \mathbf{R}(\theta(\epsilon)) \text{ with } \theta(\epsilon) = \gamma\|\boldsymbol{\psi}_\epsilon\|^2 h. \tag{5.35}$$

Keeping only those terms that are linear in ϵ gives $\mathbf{u}(t+h) = F(0)\mathbf{u}(t) + F'(0)\boldsymbol{\psi}(t)$. The result now follows as $F'(\epsilon) = F(\epsilon)\mathbf{J}\theta'(\epsilon)$ and $\theta'(\epsilon) = 2\gamma h\boldsymbol{\psi}(t)^T\mathbf{u}(t) + 2\epsilon\|\mathbf{u}(t)\|^2$. ∎

PROPOSITION 5.5. *The solution operator for the term*

$$\partial_t \mathbf{u} = [\mathcal{L} + g(\boldsymbol{\psi})\mathcal{K} + \mathcal{P}(\boldsymbol{\psi})]\,\mathbf{u} \tag{5.36}$$

in the linearized equation (3.3) *is given in the Fourier domain by*

$$\widehat{\mathbf{u}}(t+h/2,\omega) = e^{a(\omega)G(t,t+h/2)}\,\mathbf{R}(b(\omega)h/2)\left[a(\omega)\widehat{\boldsymbol{\psi}}(t,\omega)\,\frac{\partial G}{\partial u} \;+\; \widehat{\mathbf{u}}(t,\omega)\right], \tag{5.37}$$

where the directional derivative of nonlocal gain is given by

$$\frac{\partial G}{\partial u} = \frac{h}{2}\left(\frac{\partial g}{\partial u} + \frac{h}{4}\frac{\partial g_2}{\partial u}\right) \;+\; \mathcal{O}(h^3) \tag{5.38}$$

with

$$\frac{\partial g}{\partial u} = \frac{-2g^2(\boldsymbol{\psi})}{g_0 E_{\text{sat}}}\,\langle\boldsymbol{\psi},\mathbf{u}\rangle \tag{5.39}$$

and

$$\frac{\partial g_2}{\partial u} = \frac{-2g(\boldsymbol{\psi})}{g_0 E_{\text{sat}}}\left[2g^2(\boldsymbol{\psi})\,\langle\mathcal{K}\boldsymbol{\psi},\mathbf{u}\rangle \;+\; (3g(\boldsymbol{\psi})\,\langle\mathcal{K}\boldsymbol{\psi},\boldsymbol{\psi}\rangle + 2\langle\boldsymbol{\psi},\mathcal{L}\boldsymbol{\psi}\rangle)\frac{\partial g}{\partial u}\right]. \tag{5.40}$$

Remark. The inner products in (5.39) and (5.40) are the L^2-inner products $\langle\cdot,\cdot\rangle = \langle\cdot,\cdot\rangle_{L^2(\mathbb{R},\mathbb{C}^2)}$. These can be computed in the frequency domain using the formulae

$$\langle\mathcal{K}\boldsymbol{\psi},\mathbf{u}\rangle = \int_{-\infty}^{\infty} a(\omega)\,\widehat{\boldsymbol{\psi}}^*(\omega)\,\widehat{\mathbf{u}}(\omega)\,d\omega, \tag{5.41}$$

$$\langle\mathcal{K}\boldsymbol{\psi},\boldsymbol{\psi}\rangle = \int_{-\infty}^{\infty} a(\omega)\,\|\widehat{\boldsymbol{\psi}}(\omega)\|^2\,d\omega, \tag{5.42}$$

$$\langle\boldsymbol{\psi},\mathcal{L}\boldsymbol{\psi}\rangle = \int_{-\infty}^{\infty} b(\omega)\,\widehat{\boldsymbol{\psi}}^*(\omega)\,\mathbf{J}\,\widehat{\boldsymbol{\psi}}(\omega)\,d\omega. \tag{5.43}$$

∎

Proof. The proof is similar to that of Proposition 5.4. Let $G(\boldsymbol{\psi}, h) = G(t, t+h)$ as in (5.28). This time, we set $F(\epsilon)(\omega) = e^{a(\omega)G(\epsilon,h)}\,\mathbf{R}(b(\omega)h/2)$, where $G(\epsilon, h) = G(\boldsymbol{\psi} + \epsilon\mathbf{u}, h)$. Then $F'(\epsilon) = a(\omega)\partial_\epsilon G(\epsilon, h)\,F(\epsilon)$. Therefore, (5.37) follows by defining $\frac{\partial G}{\partial u} = \partial_\epsilon G(0, h)$, in accordance with the definition of the directional derivative.

Next, (5.38) follows from (5.29), where

$$\frac{dg}{du} := \left.\frac{\partial}{\partial\epsilon}\right|_{\epsilon=0} g(\boldsymbol{\psi} + \epsilon\mathbf{u}) = \frac{-g^2(\boldsymbol{\psi})}{g_0 E_{\rm sat}}\frac{\partial E}{\partial u} = \frac{-2g^2(\boldsymbol{\psi})}{g_0 E_{\rm sat}}\langle\boldsymbol{\psi}, \mathbf{u}\rangle, \tag{5.44}$$

and $\frac{dg_2}{du}$ is calculated as follows. First, as functions of x, we have that

$$g_2(\boldsymbol{\psi}) = F_1(\boldsymbol{\psi})F_2(\boldsymbol{\psi}), \tag{5.45}$$

where

$$F_1(\boldsymbol{\psi}) = \frac{-2g^2(\boldsymbol{\psi})}{g_0 E_{\rm sat}} \quad \text{and} \quad F_2(\boldsymbol{\psi}) = \langle\boldsymbol{\psi}, (\mathcal{L} + g(\boldsymbol{\psi})\mathcal{K})\boldsymbol{\psi}\rangle. \tag{5.46}$$

Now

$$\frac{\partial F_1}{\partial u} = \frac{-4g(\boldsymbol{\psi})}{g_0 E_{\rm sat}}\frac{\partial g}{\partial u} \tag{5.47}$$

and

$$\frac{\partial F_2}{\partial u} = \langle\mathbf{u}, (\mathcal{L} + g(\boldsymbol{\psi})\mathcal{K})\boldsymbol{\psi}\rangle \;+\; \langle\boldsymbol{\psi}, \mathcal{K}\boldsymbol{\psi}\rangle\frac{\partial g}{\partial u} \;+\; \langle\boldsymbol{\psi}, (\mathcal{L} + g(\boldsymbol{\psi})\mathcal{K})\mathbf{u}\rangle \tag{5.48}$$

$$= 2g(\boldsymbol{\psi})\langle\mathcal{K}\boldsymbol{\psi}, \mathbf{u}\rangle \;+\; \langle\boldsymbol{\psi}, \mathcal{K}\boldsymbol{\psi}\rangle\frac{\partial g}{\partial u} \tag{5.49}$$

since $\mathcal{K}^* = \mathcal{K}$ and $\mathcal{L}^* = -\mathcal{L}$. Equation (5.40) now follows by applying the product rule to (5.45). ∎

5.4. Solution operators for the adjoint linearized equations. In this subsection, we describe the split-step method we used to solve the adjoint linearized equation in the fiber amplifier, which is not completely straightforward due to the nonlocal saturable gain g.

Since the adjoint linearized equation in a fiber segment is solved backward in time, we introduce the backward time variable $s = L - t$, where L is the length of the segment. By (4.7), in the fiber amplifier, the adjoint equation is given by

$$\partial_s\mathbf{v} = \left(\mathcal{L}^T + g(\boldsymbol{\psi}(t))\mathcal{K}^T + [\mathcal{M}_1(\boldsymbol{\psi}(t))]^T + [\mathcal{M}_2(\boldsymbol{\psi}(t))]^T + [\mathcal{P}(\boldsymbol{\psi}(t))]^T\right)\mathbf{v}, \tag{5.50}$$

where $\mathcal{L}$ and $\mathcal{M}_1$ are antisymmetric, $\mathcal{K}$ is symmetric, and $\mathcal{M}_2^T = -2\gamma\boldsymbol{\psi}\boldsymbol{\psi}^T\mathbf{J}$. Next, we recall from (3.5) that $\mathcal{P}(\mathbf{u}) = \frac{-2g^2}{g_0 E_{\rm sat}}\mathcal{K}\boldsymbol{\psi}\,\langle\boldsymbol{\psi}, \mathbf{u}\rangle$. A calculation based on the defining formula for the adjoint (4.11) shows that

$$\mathcal{P}^T(\mathbf{v}) = \frac{-2g^2}{g_0 E_{\rm sat}}\boldsymbol{\psi}\,\langle\mathcal{K}\boldsymbol{\psi}, \mathbf{v}\rangle. \tag{5.51}$$

PROPOSITION 5.6. *The solution operator for the adjoint equation* (5.50) *in a fiber amplifier of length L is given up to terms of order $\mathcal{O}(h^3)$ by*

$$\begin{aligned}\mathbf{v}(s) &= \mathcal{U}^*(s, s-h)\mathbf{v}(s-h)\\ &= [\exp(\mathcal{A}(t+h/2, t))]^*\,[\exp(\mathcal{B}(t+h, t))]^*\,[\exp(\mathcal{A}(t+h, t+h/2))]^*,\end{aligned} \tag{5.52}$$

where $t = L - s$, and the split solution operators are given by

$$[\exp(\mathcal{B}(t+h,t))]^* = (\mathbf{I} - 2\gamma\boldsymbol{\psi}(t)\boldsymbol{\psi}(t)^T\mathbf{J})\,\mathbf{R}(-\gamma\|\boldsymbol{\psi}(t)\|^2 h), \tag{5.53}$$

which is most readily computed in the fast-time domain, and

$$\begin{aligned}[\exp(\mathcal{A}(t+h/2,t))]^*\mathbf{v} &= \nabla G(h/2)\,\langle \mathcal{K}\boldsymbol{\psi}(t), \mathbf{w}\rangle + \mathbf{w},\\ \mathbf{w} &= \exp\left[-\mathcal{L}h/2 + G(\boldsymbol{\psi}(t), h/2)\mathcal{K}\right]\,\mathbf{v},\end{aligned} \tag{5.54}$$

which is most readily computed in the frequency domain. Here

$$\nabla G(\boldsymbol{\psi}, h/2) = \frac{h}{2}\left[\alpha_1\boldsymbol{\psi} + \frac{h}{4}(\alpha_2\mathcal{K}\boldsymbol{\psi} + \alpha_3\boldsymbol{\psi})\right], \tag{5.55}$$

where

$$\alpha_1 = \frac{-2g^2}{g_0 E_{\rm sat}}, \qquad \alpha_2 = 2g\alpha_1, \qquad \alpha_3 = \frac{-2g}{g_0 E_{\rm sat}}\left(3g\langle\mathcal{K}\boldsymbol{\psi},\boldsymbol{\psi}\rangle + 2\langle\boldsymbol{\psi},\mathcal{L}\boldsymbol{\psi}\rangle\right)\alpha_1 \tag{5.56}$$

are all evaluated at time t.

Proof. We recall from (5.19) that the solution operator for the linearized equation from time t to $t+h$ is of the form

$$\begin{aligned}\mathbf{u}(t+h) &= \mathcal{U}(t+h,t)\,\mathbf{u}(t)\\ &= \exp(\mathcal{A}(t+h,t+h/2))\exp(\mathcal{B}(t+h,t))\exp(\mathcal{A}(t+h/2,t))\;\mathbf{u}(t),\end{aligned} \tag{5.57}$$

where the operators $\mathcal{A}$ and $\mathcal{B}$ are given in Propositions 5.4 and 5.5, respectively. Since the forward time interval $[t, t+h]$ corresponds to the backward time interval $[s-h, s]$, the solution operator for the adjoint equation is given by

$$\mathbf{v}(s) = \mathcal{U}^*(s, s-h)\mathbf{v}(s-h) = [\mathcal{U}(t+h,t)]^*\mathbf{v}(s-h), \tag{5.58}$$

from which we obtain (5.52). To establish (5.54), we first observe that the gradient ∇G is defined so that $\frac{\partial G}{\partial u} = \langle \nabla G, \mathbf{u}\rangle$. Then, as in (5.37),

$$\mathbf{u}(t+h) = \exp(A(t+h/2,t))\;\mathbf{u}(t) = \exp(\mathcal{L}h/2 + G(\boldsymbol{\psi}, h/2)\mathcal{K})\;(\mathbf{u}(t) + \mathcal{K}\boldsymbol{\psi}\langle\nabla G, \mathbf{u}\rangle).$$

Equation (5.54) now follows from the identity $\langle \mathcal{T}(\mathbf{f}\langle\mathbf{g},\mathbf{u}\rangle), \mathbf{v}\rangle = \langle \mathbf{u}, \langle \mathbf{f}, \mathcal{T}^*\mathbf{v}\rangle\mathbf{g}\rangle$. ∎

6. Spectrum of the monodromy operator. In analogy with the Floquet theory of periodic solutions of nonlinear ODEs [44], we expect that the stability of a periodically stationary pulse solution, $\boldsymbol{\psi}$, of a lumped laser model can be determined by the spectrum $\sigma(\mathcal{M})$ of the monodromy operator. The spectrum of $\mathcal{M}$ is the union of the essential spectrum $\sigma_{\rm ess}(\mathcal{M})$ and the eigenvalues [53]. In [38, 39], we derived a formula for $\sigma_{\rm ess}(\mathcal{M})$. As in [7, 39], we approximate $\sigma(\mathcal{M})$ by the set of eigenvalues of a matrix approximation, $\mathbf{M}$, of the operator $\mathcal{M} : L^2(\mathbb{R},\mathbb{R}^2) \to L^2(\mathbb{R},\mathbb{R}^2)$. To do so, we first truncate the domain $\mathbb{R}$ to a finite interval, which we then discretize using N equally spaced points, x_j. Then any function $\boldsymbol{\psi} = (\psi_1, \psi_2)^T \in L^2(\mathbb{R},\mathbb{R}^2)$ is approximated by a vector $[\psi_1(x_0), \psi_2(x_0), \cdots, \psi_1(x_{N-1}), \psi_2(x_{N-1}]^T \in \mathbb{R}^{2N}$. As a consequence, the operator $\mathcal{M}$ can be approximated by a linear transformation $\mathbb{M} : \mathbb{R}^{2N} \to \mathbb{R}^{2N}$. To compute the matrix $\mathbf{M}$ of $\mathbb{M}$ in the standard basis, we recall that for each $k \in \{1, \cdots, 2N\}$, the kth column of $\mathbf{M}$ is given by the action of $\mathbb{M}$ on the kth standard basis vector $\mathbf{e}_k \in \mathbb{R}^{2N}$. That is, using (3.1), the kth column of $\mathbf{M}$ is obtained

by numerically solving the linearized equations given in section 3 for one round trip of the laser with an initial condition given by $\mathbf{e}_k$.

In the remainder of this section, we present some theoretical results about the spectrum of $\mathcal{M}$. The linear stability of a stationary pulse solution of the NLSE is determined by the spectrum of the linearized differential operator $\mathcal{L}$. It is well known that $\mathcal{L}$ has an eigenvalue with algebraic multiplicity four at $\lambda = 0$, which is due to the phase and fast-time translation invariances of the NLSE [21]. In this section, we will show that a minor modification of the monodromy operator has a multiplicity two eigenvalue at $\lambda = 1$. As in the case of the NLSE, these eigenvalues are due to the phase and time translation invariances of the lumped laser model. In analogy with a result of Haus and Mecozzi [16] for stationary pulses, we expect that perturbations which couple into the corresponding eigenfunctions will result in shifts in the phase and position of the pulse [16]. A result of Lunardi for periodic solutions of nonlinear parabolic equations [27] suggests that, except for such phase and time shifts, a periodically stationary pulse solution of the lumped model will behave stably if $\sup\{|\lambda| : \lambda \in \sigma(\mathcal{M}), \lambda \neq 1\} < 1$. However, we leave the precise formulation and proof of such a result to a future paper.

We recall that a pulse, $\boldsymbol{\psi}$, is periodically stationary if $\mathcal{R}(\psi) = \mathbf{R}(\theta)\psi$ for some θ and that the optimization method in section 4 computes the pair $(\boldsymbol{\psi}, \theta)$. Since Floquet theory only applies to solutions that are actually periodic, we absorb the constant rotation $\mathbf{R}(\theta)$ into $\mathcal{R}$ by defining a *modified roundtrip operator* by $\widetilde{\mathcal{R}} := \mathbf{R}(-\theta) \circ \mathcal{R}$ so that $\widetilde{\mathcal{R}}\boldsymbol{\psi} = \boldsymbol{\psi}$. We also have a *modified monodromy operator,* $\widetilde{\mathcal{M}} := \mathbf{R}(-\theta) \circ \mathcal{M}$.

PROPOSITION 6.1. *Let $\boldsymbol{\psi}$ be a periodically stationary pulse with $\mathcal{R}\boldsymbol{\psi} = \mathbf{R}(\theta)\boldsymbol{\psi}$, and suppose that $\boldsymbol{\psi}, \boldsymbol{\psi}_x \in L^2(\mathbb{R}, \mathbb{R}^2)$. Let*

$$\mathbf{u}_{\rm ph} = \mathbf{J}\boldsymbol{\psi} \tag{6.1}$$

be the $\pi/2$-rotation of $\boldsymbol{\psi}$, and let

$$\mathbf{u}_{\rm tr} = \boldsymbol{\psi}_x \tag{6.2}$$

be the x-derivative of $\boldsymbol{\psi}$. Let $\widetilde{\mathcal{M}} = \mathbf{R}(-\theta) \circ \mathcal{M}$ be the modified monodromy operator. Then

$$\widetilde{\mathcal{M}}\,\mathbf{u}_{\rm ph} = \mathbf{u}_{\rm ph} \qquad \textit{and} \qquad \widetilde{\mathcal{M}}\,\mathbf{u}_{\rm tr} = \mathbf{u}_{\rm tr}. \tag{6.3}$$

Consequently, $\lambda = 1$ is an eigenvalue of $\widetilde{\mathcal{M}}$ with multiplicity (at least) two.

Remark. We call $\mathbf{u}_{\rm ph}$ the phase invariance eigenfunction and $\mathbf{u}_{\rm tr}$ the translation invariance eigenfunction. We note that the $\mathcal{M}$ itself does not generically have any eigenvalues on the unit circle. ∎

Remark. The NLSE has the soliton solution

$$\psi(t,x) = A\,\mathrm{sech}\{A\,[x - x_0 + \Omega t]\}\,\exp\left\{i\left[\Phi + \frac{1}{2}\left(A^2 - \Omega^2\right)t - \Omega x\right]\right\}. \tag{6.4}$$

Just as in Proposition 6.1, the phase and fast-time invariances of the NLSE give rise to two eigenvalues at zero with eigenfunctions given by ψ_Φ and ψ_{x_0}, respectively. (Here ψ_p denotes the partial derivative of ψ with respect to a parameter, p.) In addition, if $\mathcal{L}$ denotes the linearized operator, then $\mathcal{L}\psi_A = A\psi_\Phi$ and $\mathcal{L}\psi_\Omega = A\psi_{x_0}$, which gives rise to two Jordan blocks, one associated with $\{\psi_\Phi, \psi_A\}$ and the second with $\{\psi_{x_0}, \psi_\Omega\}$ [21].

Consequently, $\lambda = 0$ is an eigenvalue with algebraic multiplicity four. From another perspective, for the NLSE, $\mathcal{L}$ is a real Hamiltonian operator, which implies that if λ is an eigenvalue, then so are $-\lambda$ and $\pm\overline{\lambda}$ [22]. However, in our situation, although the monodromy operator $\mathcal{M}$ is real, it is not Hamiltonian, and the Jordan blocks involving the amplitude and frequency eigenfunctions do not exist. Consequently, the eigenvalue at $\lambda = 1$ only has algebraic multiplicity two. Furthermore, we recall that when one linearizes an autonomous ODE about a time-periodic solution, the resulting monodromy operator always has an eigenvalue $\lambda = 1$ due to the time invariance of the nonlinear equation [44]. In the context of the Kuznetsov–Ma breather solution of the NLSE, this corresponds to an additional pair of eigenvalues at $\lambda = 1$ [7]. However, this phenomenon does not occur in our context, as the lumped model we are studying is not autonomous. ∎

Proof. First, let $\boldsymbol{\psi}_\epsilon$ be the perturbation of $\boldsymbol{\psi}$ given by the phase rotation $\boldsymbol{\psi}_\epsilon = \mathbf{R}(\epsilon)\boldsymbol{\psi}_0$, and let $\mathbf{u} := \lim_{\epsilon\to 0} \frac{\boldsymbol{\psi}_\epsilon - \boldsymbol{\psi}}{\epsilon}$. Then $\mathbf{u} = \mathbf{R}'(0)\boldsymbol{\psi} = \mathbf{J}\boldsymbol{\psi}_0$ is a $\pi/2$-rotation of $\boldsymbol{\psi}$. On the other hand, by the phase-shift invariance of each of the nonlinear operators $\mathcal{P}$, we have that

$$\widetilde{\mathcal{M}}(\mathbf{u}) = \lim_{\epsilon\to 0} \frac{\widetilde{\mathcal{R}}(\boldsymbol{\psi}_\epsilon) - \widetilde{\mathcal{R}}(\boldsymbol{\psi})}{\epsilon} = \lim_{\epsilon\to 0} \frac{\boldsymbol{\psi}_\epsilon - \boldsymbol{\psi}}{\epsilon} = \mathbf{u}. \tag{6.5}$$

If instead we let ψ_ϵ be the time translation of $\boldsymbol{\psi}$ given by $\boldsymbol{\psi}_\epsilon(x) = \boldsymbol{\psi}(x+\epsilon)$, then $\mathbf{u} = \boldsymbol{\psi}_x$ is the x-derivative of $\boldsymbol{\psi}$, and because of the fast-time translation invariance of all the operators $\mathcal{P}$, we again obtain (6.5). ∎

Since $\widetilde{\mathcal{M}} : L^2(\mathbb{R},\mathbb{R}^2) \to L^2(\mathbb{R},\mathbb{R}^2)$ is a real operator, the elements of the spectrum either are real or come in complex conjugate pairs. In [38], we proved that under reasonable assumptions on the system parameters and on the smoothness and decay of the pulse, the essential spectrum is given by

$$\sigma_{\text{ess}}(\widetilde{\mathcal{M}}) = \{\, \lambda_\pm(\omega) \in \mathbb{C} \mid \omega \in \mathbb{R} \,\} \cup \{0\}, \tag{6.6}$$

where

$$\lambda_\pm(\omega) = \ell_{\text{OC}}(1-\ell_0) \exp\left\{ \frac{1}{2}\left(1 - \frac{\omega^2}{\Omega_g^2}\right) \int_0^{L_{\text{FA}}} g(\psi(t))dt \right\} \exp\left\{ \pm i \left(\frac{\beta_{\text{RT}}}{2}\omega^2 - \theta \right) \right\}. \tag{6.7}$$

Here $\beta_{\text{RT}} = \beta_{\text{SMF1}}\text{L}_{\text{SMF1}} + \beta_{\text{FA}}\text{L}_{\text{FA}} + \beta_{\text{SMF2}}\text{L}_{\text{SMF2}} + \beta_{\text{DCF}}$ is the roundtrip dispersion. Geometrically, $\sigma_{\text{ess}}(\mathcal{M})$ is a pair of counterrotating spirals which have a Gaussian decay in the radial direction. In [38, 39], we discuss conditions which guarantee that the essential spectrum is stable.

7. Simulation results. For the simulation results we present here, we choose the parameters in the model to be similar to those in the experimental stretched pulse laser of Kim et al. [23]. The saturable absorber is modeled by (2.9) with $\ell_0 = 0.2$ and $P_{\text{sat}} = 50$ W. The saturable absorber is followed by a segment of single-mode fiber, SMF1, modeled by (2.7) with $\gamma = 2\times 10^{-3}$ $(\text{Wm})^{-1}$, $\beta_{\text{SMF1}} = 10$ kfs^2/m, (1 $\text{kfs}^2 = 10^{-27}$ s^2), and $L_{\text{SMF1}} = 0.32$ m; a fiber amplifier, modeled by (2.4) with $g_0 = 6\text{m}^{-1}$, $E_{\text{sat}} = 200$ pJ, $\Omega_g = 50$ THz, $\gamma = 4.4\times 10^{-3}$ $(\text{Wm})^{-1}$, $\beta_{\text{FA}} = 25$ kfs^2/m, and $L_{\text{FA}} = 0.22$ m; and a second segment of single-mode fiber, SMF2, with the same parameters as SMF1 but with $L_{\text{SMF2}} = 0.11$ m. The dispersion β_{DCF} of the dispersion compensation element is chosen so that the roundtrip dispersion is $\beta_{\text{RT}} = -1$ kfs^2. Finally, the 50%

output coupler is modeled by (2.10) with $\ell_{\rm OC} = \sqrt{0.5}$. Unless otherwise stated, we used a time window $-L_X/2 \le x \le L_X/2$ of size $L_X = 10$ ps discretized with $N = 512$ points.

The algorithms were implemented in MATLAB. We used the quasi-Newton BFGS algorithm [51] as implemented in the function fminunc to find the optimal pulse. In particular, the optimization algorithm is provided with the gradient of the objective function, computed using the adjoint state method described in Theorem 4.1. The computational time to perform the optimization and compute the monodromy matrix $\mathbf{M}$ and its spectrum on a 3.5-GHz Macbook Pro is about 3 minutes. The computation of $\mathbf{M}$ was done in parallel using 12 processors.

We begin by discussing the accuracy of the numerical solvers for the roundtrip operator $\mathcal{R}$ and the linearization $\mathcal{M}$ of $\mathcal{R}$. For these results, we use two error measures: the absolute error

$$\mathcal{E}_{\rm abs}(\boldsymbol{\psi}_{\rm approx}, \boldsymbol{\psi}_{\rm exact}) = \left[\int \|\boldsymbol{\psi}_{\rm approx}(x) - \boldsymbol{\psi}_{\rm exact}(x)\|_{\mathbb{R}^2}^2 \, dx \right]^{1/2} \tag{7.1}$$

and the relative error

$$\mathcal{E}_{\rm rel}(\boldsymbol{\psi}_{\rm approx}, \boldsymbol{\psi}_{\rm exact}) = \frac{\mathcal{E}_{\rm abs}(\boldsymbol{\psi}_{\rm approx}, \boldsymbol{\psi}_{\rm exact})}{E(\boldsymbol{\psi}_{\rm exact})^{1/2}}, \tag{7.2}$$

where the pulse energy $E(\boldsymbol{\psi}_{\rm exact})$ is given by (2.6).

For this study, we used an initial pulse, $\boldsymbol{\psi}_0$, obtained by propagating a Gaussian pulse for 10 round trips of the system. The Gaussian was given by

$$g(x) = \sqrt{P_0} \exp\left(-(x/\sigma)^2\right), \tag{7.3}$$

where $\sigma = \text{FWHM}/2\sqrt{\log 2}$. By choosing a peak power of $P_0 = 400$ W and a full width at half maximum of FWHM $= 300$ fs, we obtained a reasonable approximation, $\boldsymbol{\psi}_0$, to a periodically stationary pulse.

To assess the accuracy of the numerical solver for the roundtrip operator $\mathcal{R}$, we first computed an exact solution by propagating the initial pulse $\boldsymbol{\psi}_0$ for one round trip of the system with a step size of $\Delta t = 10^{-4}$. We then computed approximate solutions using step sizes of $\Delta t = 10^{-2}$, 5×10^{-3}, 2×10^{-3}, 10^{-3}, 5×10^{-4}, and 2×10^{-4} and computed the error between the approximate and exact solutions. In the left panel of Figure 2, we plot the absolute error in units of $\text{J}^{1/2}$ as a function of Δt. The portion of the curve with $\Delta t \ge 10^{-3}$ has a slope of 4.02 as expected for the globally fourth-order method we used. The floor below an error level of 10^{-16} is due to round-off error, primarily of the Fourier transform. The relative error is approximately 10^5 times larger than the absolute error. So, for example, $\mathcal{E}_{\rm rel} = 2.9 \times 10^{-8}$ when $\Delta t = 10^{-2}$.

In the center panel of Figure 2, we show the corresponding results for the linearized operator $\mathcal{M}$. For each choice of time step, we linearized $\mathcal{R}$ about the pulse obtained by propagating $\boldsymbol{\psi}_0$ with a step size of Δt, and we chose the initial pulse for the linearized operator to be the phase invariance eigenfunction, $\mathbf{u}_0 = i\boldsymbol{\psi}_0$. In this case, the plot also has a slope of 4.02, where $\Delta t \ge 10^{-3}$ and $\mathcal{E}_{\rm rel} = 2.9 \times 10^{-8}$ when $\Delta t = 10^{-2}$. For the translation invariance eigenfunction, $\mathbf{u}_0 = \Delta_x \boldsymbol{\psi}_0$, for $\Delta t \ge 10^{-3}$, the slope (not shown) is the same as for the phase invariance eigenfunction, but the absolute errors are about twice as large.

In the right panel of Figure 2, we show the corresponding results for the adjoint of linearized operator $\mathcal{M}^*$. For these results, we chose the initial pulse to be $\mathbf{v}_0 = \mathcal{R}(\boldsymbol{\psi}_0) - e^{i\theta}\boldsymbol{\psi}_0$, where $\boldsymbol{\psi}_0$ is computed with $\Delta t = 10^{-4}$ and θ is the angle between $\boldsymbol{\psi}_0$

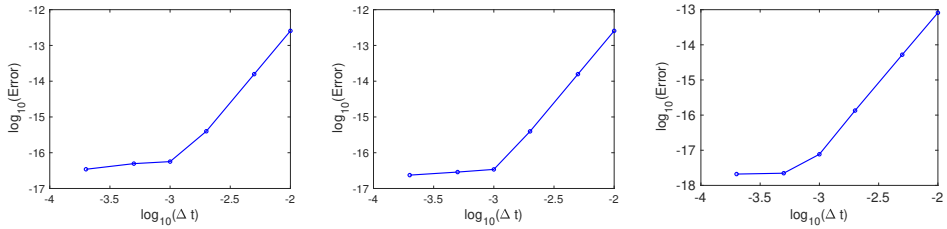

FIG. 2. *Absolute error between an exact solution (as computed with $\Delta t = 10^{-4}$) and approximate solutions with step size Δt for propagation over one round trip of the laser. Left: Result for the roundtrip operator $\mathcal{R}$. Center: Result for the linearization $\mathcal{M}$ of $\mathcal{R}$. Right: Result for the adjoint linearization $\mathcal{M}^*$.*

and $\mathcal{R}(\boldsymbol{\psi}_0)$. We note that $\max|\boldsymbol{\psi}_0| = 16.2$ and $\max|\mathbf{v}_0| = 1.2$. Once again, the plot has a slope of 4.02, where $\Delta t \geq 10^{-3}$ and $\mathcal{E}_{\text{rel}} = 8.7 \times 10^{-8}$ when $\Delta t = 10^{-2}$.

Even though the linearized roundtrip solver has the correct order of accuracy, it is nevertheless possible that the solution is not correct. To verify that the linearized roundtrip operator has been correctly derived and implemented, we must verify that

$$\mathcal{M}(\mathbf{u}_0) = \lim_{\epsilon \to 0} \frac{\mathcal{R}(\boldsymbol{\psi}_0 + \epsilon \mathbf{u}_0) - \mathcal{R}(\boldsymbol{\psi}_0)}{\epsilon} =: D_{\boldsymbol{\psi}_0}\mathcal{R}(\mathbf{u}_0). \tag{7.4}$$

If we let $f(\epsilon) := \mathcal{R}(\boldsymbol{\psi}_0 + \epsilon \mathbf{u}_0)(x) : \mathbb{R} \to \mathbb{R}^2$, then the directional derivative is given by $D_{\boldsymbol{\psi}_0}\mathcal{R}(\mathbf{u}_0)(x) = f'(0)$. Due to round-off errors, standard finite difference approximations of $f'(0)$ are not accurate when ϵ is small. A commonly employed method is to use a complex step derivative approximation [28], which requires that f is real valued. However, this is not actually the case for the numerically computed f because of small imaginary round-off errors in the computation of the discrete Fourier transforms. Instead, we use a spectral differentiation method of Fornberg [10]. With this method, Cauchy's integral formula is applied to show that if $f : \mathbb{C} \to \mathbb{C}$ is complex analytic in a disc of radius R about a point, $z_0 \in \mathbb{C}$, then for any $r \in [0, R]$,

$$f'(z_0) = \frac{1}{2\pi r} \int_0^{2\pi} F(t) e^{-it}\, dt, \tag{7.5}$$

where $F(t) = f(z_0 + re^{it})$. Then $f'(z_0) = \frac{c_1}{r}$, where c_1 is the first Fourier coefficient in the Fourier series of F. Using a discrete Fourier transform approximation with M points, we find that

$$f'(z_0) \approx \frac{1}{rM} \sum_{m=0}^{M-1} F_m w^{-m}, \tag{7.6}$$

where $w = e^{i2\pi/M}$ and $F_m = F(w^m)$.

To verify (7.4), we first extended f to a vector-valued complex analytic function $f : \mathbb{C} \to \mathbb{C}^2$ [29]. To minimize the truncation error in the discretization of the Fourier series, we need M to be sufficiently large. For the results presented here, it was sufficient to choose $M = 4$. Furthermore, to avoid round-off error in the computation of the F_m, we do not want r to be too small [5]. In the left panel of Figure 3, for the phase invariance eigenfunction $\mathbf{u}_0 = i\boldsymbol{\psi}_0$, we plot the absolute error between $\mathcal{M}(\mathbf{u}_0)$ and the spectral derivative approximation of $f'(0)$ as a function of r. The minimum error is 2.4×10^{-17} at $r = 2^{-10}$. Similar results were obtained for the translation

invariance eigenfunction $\mathbf{u}_0 = \Delta_x \boldsymbol{\psi}_0$. These results were obtained using a time step of $\Delta t = 10^{-2}$. Decreasing the time step to $\Delta t = 10^{-3}$, we obtained a similar plot, except that the minimum error increased to 7.8×10^{-17}, likely due to the larger accumulation of round-off errors in the numerical solution of the system model.

As a second test of the adjoint solver, we examine the accuracy of the computation of the directional derivative $D_{\boldsymbol{\psi}_0}\mathcal{E}(\mathbf{u}_0) = \langle \frac{\delta \mathcal{E}}{\delta \boldsymbol{\psi}_0}, \mathbf{u}_0 \rangle$, where the variational derivative $\frac{\delta \mathcal{E}}{\delta \boldsymbol{\psi}_0}$ is given in terms of the adjoint of $\mathcal{M}$ by (4.4). For simplicity, for this verification, we approximate the directional derivative using a finite difference. So that round-off errors do not dominate, we need to ensure that the directional derivative is nonzero. To ensure that the variational derivative is not too close to zero, we choose $\boldsymbol{\psi}_0$ to be a Gaussian with FWHM = 50 fs and $P_0 = 200$ W, which is not a periodically stationary pulse. In addition, we choose $\mathbf{u}_0$ so that the L^2-inner product is not zero. In the right panel of Figure 3, we show the relative error between the directional derivative computed using a finite difference with increment ϵ and the computation based on the adjoint of $\mathcal{M}$. For $\epsilon > 10^{-5}$, the slope of the error plot is 0.997, as expected for a standard finite difference, which provides strong evidence for the accuracy of the implementation of the gradient of $\mathcal{E}$.

In Figure 4 (left panel), we show the instantaneous power of the optimal pulse after the output coupler (also see Figure 1, right, for a plot showing the evolution of this pulse through the laser). The initial pulse for the optimization was obtained by evolving the Gaussian (7.3) for 10 round trips, at which point the value of the objective

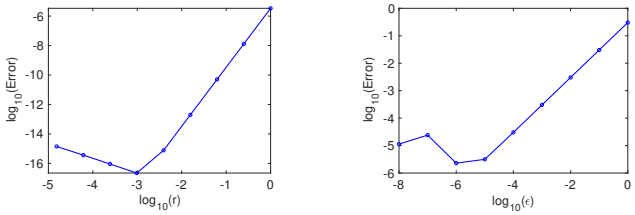

FIG. 3. *Left: Absolute error between the numerical solution of the linearized operator* $\mathcal{M}(\mathbf{u}_0)$ *and the spectral approximation of the directional derivative* $D_{\boldsymbol{\psi}_0}\mathcal{R}(\mathbf{u}_0)$ *for the theoretical phase-shift eigenfunction* $\mathbf{u}_0 = \mathbf{J}\boldsymbol{\psi}_0$. *Right: Relative error between the directional derivative of* $\mathcal{E}$ *computed in terms of the adjoint of* $\mathcal{M}$ *via* (4.3) *and* (4.4) *and using a finite difference with increment* ϵ.

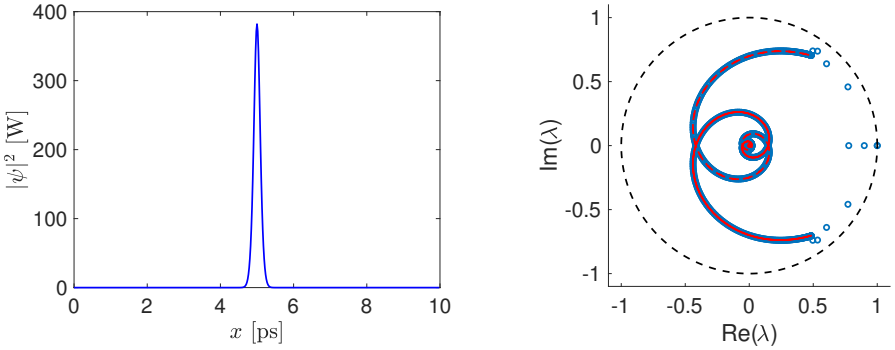

FIG. 4. *Left: Optimal pulse for the periodically stationary pulse obtained using the parameters given at the beginning of section* 7. *Right: Spectrum of the monodromy operator for the optimal pulse shown in the left panel. The eigenvalues of the discretized operator are shown with blue circles, and the essential spectrum obtained using* (6.7) *is shown with the solid red line.*

function in (4.2) was $\widetilde{\mathcal{E}} = 8 \times 10^{-3}$, which the optimization method then reduced to $\widetilde{\mathcal{E}} = 5 \times 10^{-27}$ in 36 iterations. In Figure 4 (right panel), we show the numerically computed spectrum of the modified monodromy operator $\widetilde{\mathcal{M}}$ with blue circles. A portion of this spectrum agrees with the essential spectrum obtained using (6.7), which is shown with the solid red line. In addition, counting multiplicities, there are 12 eigenvalues that are not part of the essential spectrum. We label them $\lambda_1, \cdots, \lambda_{12}$ in order of decreasing magnitude. First, there is a multiplicity two eigenvalue at $\lambda = 1$, which agrees with the theoretical predictions in Proposition 6.1. The error in the phase invariance eigenvalue is 10^{-13}, while that in the translation invariance eigenvalue is 4×10^{-11}. In Figure 5, we plot the amplitude $A(x) := \|\mathbf{u}(x)\|_{\mathbb{R}^2}$ of the corresponding phase invariance eigenfunction (left panel) and translation invariance eigenfunction (right panel). The numerically computed eigenfunctions are shown with blue dots, and the (normalized) theoretical eigenfunctions in Proposition 6.1 are shown with black solid lines. The excellent agreement with both the essential spectrum and the theoretically predicted eigenvalues and eigenfunctions at $\lambda = 1$ provides strong validation of the numerical method.

There are two additional eigenvalues on the real axis at $\lambda_5 = 0.8987$ and $\lambda_{12} = 0.7773$. The amplitude of the eigenfunction corresponding to λ_5, which is shown with the red-dashed line in the right panel of Figure 5, is very similar to the translation invariance eigenfunction. Similarly, the eigenfunction corresponding to λ_{12}, which is shown with the red-dashed line in the left panel of Figure 5, is very similar to the phase invariance eigenfunction. Finally, there are four eigenvalues near the edge of the upper arm of the essential spectrum. The corresponding eigenfunctions are shown in Figure 6. We observe that the number of oscillations in the amplitude of these eigenfunctions increases as the distance from the eigenvalue to the edge of the essential spectrum decreases.

To investigate the extent of the region in parameter space where stable pulses exist, we performed three parameter continuation studies. In [39], we reported on how the parameters in the saturable absorber affect the essential spectrum. Here we focus on the parameters in the fiber amplifier. Starting from the system parameters given above, we first increased the unsaturated gain from $g_0 = 6$ to $g_0 = 7$ in increments of 0.1. During this parameter continuation, the peak power of the pulse increased

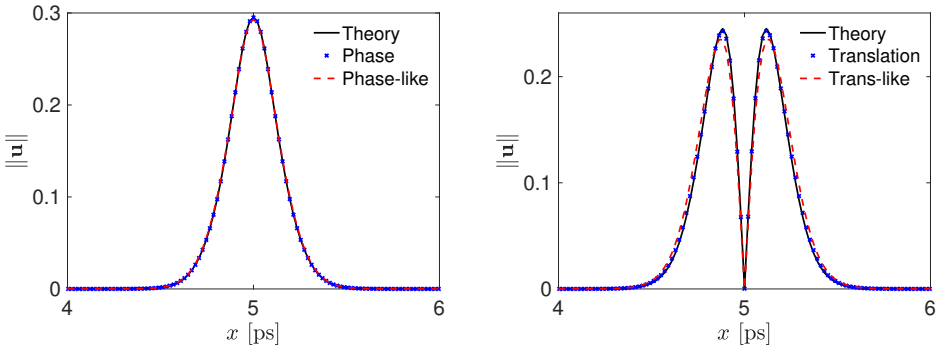

FIG. 5. *Left: Phase invariance eigenfunctions: theoretical (black solid line) and numerical (blue dots) eigenfunctions with* $\lambda = 1$ *and numerical eigenfunction corresponding to* $\lambda = 0.7773$ *(red dashed line). Right: Translation invariance eigenfunctions: theoretical (black solid line) and numerical (blue dots) eigenfunctions with* $\lambda = 1$ *and numerical eigenfunction corresponding to* $\lambda = 0.8987$ *(red dashed line).*

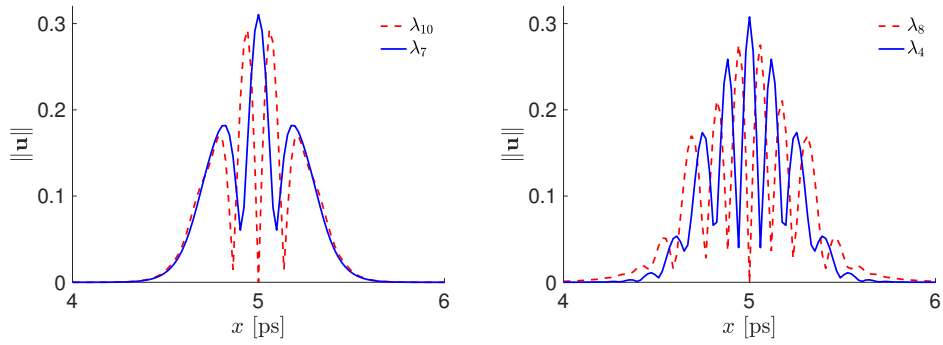

FIG. 6. *Left: Eigenfunctions corresponding to the eigenvalues* $\lambda_{10} = 0.6040 + 0.6393i$ *and* $\lambda_7 = 0.7711 + 0.4587i$. *Right: Eigenfunctions corresponding to the eigenvalues* $\lambda_8 = 0.4961 + 0.7397i$ *and* $\lambda_4 = 0.5335 + 0.7379i$, *which are the closest and the next to closest to the edge of the upper arm of the essential spectrum.*

linearly from 382 to 493 W, and the root mean square (RMS) pulse width increased linearly from 95 to 108 fs. In the left panel of Figure 7, we show the essential spectrum at the final value $g_0 = 7$. In general, the edge of the upper arm of the essential spectrum is located at $\lambda_+(0)$, where $\lambda_+(\omega)$ is given in (6.7). In particular, $|\lambda_+(0)|$ is determined by the balance of saturable gain and loss in the system, and $\arg(\lambda_+(0)) = \theta$ is the optimized phase angle in (4.1). Just as for the standard soliton, as the peak power of the pulse increases (due to the increase in g_0), the angle θ increases, rotating the upper arm of the essential spectrum counterclockwise. In addition, the four complex eigenvalues in the first quadrant rotate in the same direction, approximately maintaining their distance from the unit circle. Significantly, at $g_0 = 7$, there is a fifth eigenvalue located just above $\lambda_+(0)$. This eigenvalue bifurcates out of the edge of the essential spectrum when $g_0 = 6.5$. Finally, the phase-like eigenvalue moves slightly in, and the translation-like eigenvalue does not move.

Next, returning to the original set of parameters, we increased the saturation energy from $E_{\text{sat}} = 200$ to $E_{\text{sat}} = 260$ pJ in increments of 5 pJ. The peak power of the pulse increased linearly from 382 to 461 W, and the RMS pulse width increased linearly from 95 to 104 fs. In the right panel of Figure 7, we show the essential spectrum at $E_{\text{sat}} = 260$ pJ. Qualitatively, the same changes occur in the spectrum as when we increased g_0, except that the amount of rotation is not quite as large since the final peak power is lower.

Finally, we increased the fiber amplifier bandwidth from $\Omega_g = 50$ to $\Omega_g = 145$ THz in increments of 0.5 THz and then jumped to $\Omega_g = 500$ THz. During this parameter continuation, the peak power decreased from 382 to 379 W at $\Omega_g = 70$ THz and then increased to 382 W at $\Omega_g = 500$ THz. The RMS pulse width increased from 95 to 110 fs. In the left panel of Figure 8, we show the essential spectrum at $\Omega_g = 500$ THz. Although the peak power does not change much, the wider filter still results in a more nonlinear system, which results in θ increasing from 56° to 67°. In addition, the essential spectrum spirals much more slowly into the origin (we only show the first few rotations in the red curves). We also see that the translation-like eigenvalue on the real axis has moved out to $\lambda = 0.999$, while the phase-like eigenvalue moves inward slightly, crossing the expanding essential spectrum curve. Meanwhile, the four discrete eigenvalues in the first quadrant move outward toward the unit circle, slowing down significantly once $\Omega_g > 140$ THz. In the right panel, we see that once $\Omega_g = 65$

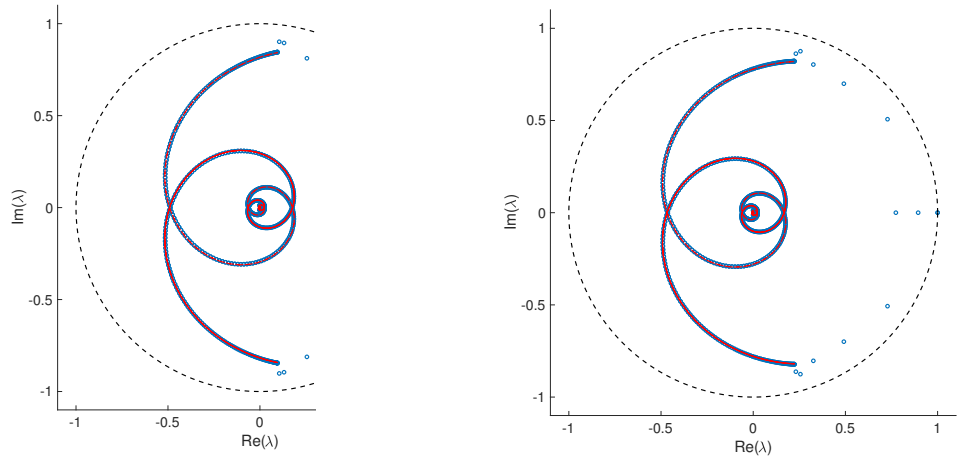

FIG. 7. *Spectra of the monodromy operator for $q_0 = 7$ (left) and $E_{\text{sat}} = 260$ pJ (right).*

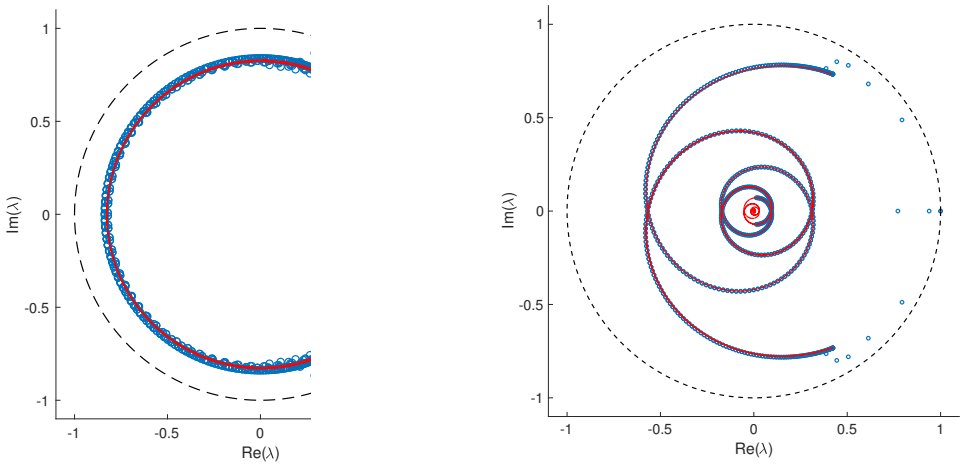

FIG. 8. *Spectra of the monodromy operator for $\Omega_g = 500$ THz (left) and $\Omega_g = 65$ THz (right).*

THz, a fifth eigenvalue has bifurcated out of the essential spectrum. In the left panel of Figure 9, we see this eigenvalue emerging from the essential spectrum at $\Omega_g = 60$ THz, slightly behind the edge.

For stationary pulses, it is well known [4, 6] that there can be significant errors when the spectrum of the linearized operator $\mathcal{L}$ is approximated by the set of eigenvalues of a matrix approximation, $\mathbf{L}$. Specifically, if an eigenfunction decays very slowly, there can be a large error in the corresponding eigenvalue due to windowing effects. This phenomenon only occurs for eigenvalues that are sufficiently close to the essential spectrum. In addition, the portion of the spectrum of $\mathbf{L}$ that corresponds to the essential spectrum may not agree with an analytical formula for $\sigma_{\text{ess}}(\mathcal{L})$. For the eigenvalues of $\mathcal{L}$, the issue can be resolved by using computational Evans function methods [6, 17] or by the iterative solution of an appropriately formulated nonlinear eigenproblem [37, 48]. However, for periodically stationary pulses, even those obtained as solutions of constant coefficient nonlinear wave equations, there is currently no numerical method for addressing this problem. Although it is no guarantee of

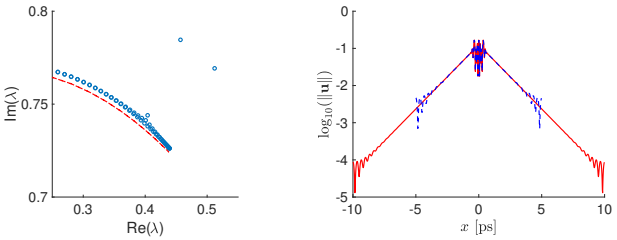

FIG. 9. *Left: Detail of the spectrum near the upper arm of the essential spectrum for* $\Omega_g = 60\ THz$. *Right: Eigenfunction corresponding to the eigenvalue that bifurcates out of the essential spectrum on the left computed using* $L = 10\ ps$, $N = 512$ *(blue dashed line) and* $L = 20\ ps$, $N = 1024$ *(red solid line).*

accuracy, the best one can do is to double the time window L and the number of points N and look for changes in the location of the eigenvalues near the essential spectrum and in the decay rates of the corresponding eigenfunctions. Indeed, we verified that the location of the eigenvalue bifurcating out of the essential spectrum in the left panel of Figure 9 does not change, and, as we see in the right panel, neither does the decay rate of the corresponding eigenfunction. In the left panel, we do, however, see some discrepancy between the analytic formula for the essential spectrum and its discrete approximation. Similar differences occur near the edge of the essential spectrum for all the simulations we performed. However, they are only evident on the larger scale in the left panel of Figure 8.

8. Conclusions. In this paper, we described and validated accurate and efficient computational methods to discover periodically stationary pulses in a lumped model of a fiber laser and to assess their stability using the spectrum of a monodromy operator. In particular, we demonstrated excellent agreement between the numerically computed spectrum on the one hand and theoretical formulae for the essential spectrum and a multiplicity two eigenvalue on the other. Our simulations suggest that there is a large region in the parameter space of the fiber amplifier in which the Kim laser operates stably. An advantage of the spectral approach to stability over the traditional evolution approach used in the engineering community is that changes in the spectrum can be used to predict the onset of an instability. However, an unresolved theoretical problem is to establish a result relating spectral stability to linear stability in this context.

To be useful for quantitative modeling of experimental lasers, the methods described here need to be extended to more realistic models of saturable absorbers (semiconductor saturable absorber mirrors) [30] and to erbium-doped fiber amplifiers modeled by multilevel rate equations [12]. In particular, we plan to apply our approach to the Mamyshev oscillator [36, 40, 43], which has extremely large pulse variations in which one-half of the pulse is destroyed each round trip before being regenerated. As is well appreciated by practitioners in the field, a major challenge of optimizing for stationary and periodically stationary pulses is the need for very good initial guesses. Further research on parameter continuation methods for pulse solutions of nonlinear wave equations and lumped models is required to address this challenge [46]. In addition, since the majority of computational time is devoted to computing the monodromy matrix, it may prove advantageous to employ a matrix-free iterative method to compute only the handful of eigenvalues that are not already identified by the theory.

A major challenge in the modeling of fiber lasers is to quantify the effects that quantum mechanical and technical noise sources have on the performance of the system [34, 35]. Traditionally, this has been accomplished using theory for idealized models and highly computationally intensive Monte Carlo simulations for more realistic ones. Building on classical results of soliton perturbation theory, Menyuk and Wang have shown how to efficiently quantify the system performance of stationary pulses in an averaged laser model by integration of the noise probability density function against numerically computed eigenfunctions [30]. An important next step is to extend this approach to periodic stationary pulses.

Acknowledgments. We thank Y. Latushkin, J. Marzuola, C. R. Menyuk, and S. Wang for generously sharing their expertise with us. The authors acknowledge computational resources provided by the Office of Information Technology Cyberinfrastructure Research Computing (CIRC) at The University of Texas at Dallas. Finally, we thank the reviewers for their comments which improved the paper.

REFERENCES

[1] G. P. Agrawal, *Nonlinear Fiber Optics*, Elsevier, New York, 2006.
[2] D. M. Ambrose and J. Wilkening, *Computing time-periodic solutions of nonlinear systems of partial differential equations*, in Hyperbolic Problems: Theory, Numerics and Applications, World Scientific, River Edge, NJ, 2012, pp. 273–280.
[3] W. Bao, S. Jin, and P. A. Markowich, *On time-splitting spectral approximations for the Schrödinger equation in the semiclassical regime*, J. Comput. Phys., 175 (2002), pp. 487–524.
[4] I. Barashenkov and E. Zemlyanaya, *Oscillatory instabilities of gap solitons: A numerical study*, Comput. Phys. Commun., 126 (2000), pp. 22–27.
[5] S. Boisgérault, *Complex Analysis and Applications*, https://eul.ink/complex-analysis, 2019.
[6] T. J. Bridges, G. Derks, and G. Gottwald, *Stability and instability of solitary waves of the fifth-order KdV equation: A numerical framework*, Phys. D, 172 (2002), pp. 190–216.
[7] J. Cuevas-Maraver, P. G. Kevrekidis, D. J. Frantzeskakis, N. I. Karachalios, M. Haragus, and G. James, *Floquet analysis of Kuznetsov-Ma breathers: A path towards spectral stability of rogue waves*, Phys. Rev. E, 96 (2017), 012202.
[8] S. A. Diddams, *The evolving optical frequency comb*, J. Opt. Soc. Am. B, 27 (2010), pp. B51–B62.
[9] M. E. Fermann, V. I. Kruglov, B. C. Thomsen, J. M. Dudley, and J. D. Harvey, *Self-similar propagation and amplification of parabolic pulses in optical fibers*, Phys. Rev. Lett., 84 (2000), pp. 6010–6013.
[10] B. Fornberg, *Numerical differentiation of analytic functions*, ACM Trans. Math. Software, 7 (1981), pp. 512–526.
[11] W. Fu, L. G. Wright, P. Sidorenko, S. Backus, and F. W. Wise, *Several new directions for ultrafast fiber lasers*, Opt. Express, 26 (2018), pp. 9432–9463.
[12] R. Giles and E. Desurvire, *Modeling erbium-doped fiber amplifiers*, J. Lightwave Technol., 9 (1991), pp. 271–283.
[13] I. Hartl, T. R. Schibli, A. Marcinkevicius, D. C. Yost, D. D. Hudson, M. E. Fermann, and J. Ye, *Cavity-enhanced similariton Yb-fiber laser frequency comb:* 3×10^{14} *W/cm*^{2} *peak intensity at* 136 *MHz*, Opt. Lett., 32 (2007), pp. 2870–2872.
[14] H. A. Haus, *Theory of mode locking with a fast saturable absorber*, J. Appl. Phys., 46 (1975), pp. 3049–3058.
[15] H. A. Haus, *Mode locking of lasers*, IEEE J. Sel. Top. Quantum Electron., 6 (2000), pp. 1173–1185.
[16] H. A. Haus and A. Mecozzi, *Noise of mode-locked lasers*, J. Quantum Electron., 29 (1993), pp. 983–996.
[17] J. Humpherys and J. Lytle, *Root following in Evans function computation*, SIAM J. Numer. Anal., 53 (2015), pp. 2329–2346.
[18] T. Kapitula, N. Kutz, and B. Sandstede, *The Evans function for nonlocal equations*, Indiana Univ. Math. J., 53 (2004), pp. 1095–1126.
[19] T. Kapitula and B. Sandstede, *Instability mechanism for bright solitary-wave solutions to the cubic-quintic Ginzburg-Landau equation*, J. Opt. Soc. Am. B, 15 (1998), pp. 2757–2762.

[20] T. Kapitula and B. Sandstede, *Stability of bright solitary-wave solutions to perturbed nonlinear Schrödinger equations*, Phys. D, 124 (1998), pp. 58–103.
[21] D. Kaup, *Perturbation theory for solitons in optical fibers*, Phys. Rev. A, 42 (1990), pp. 5689–5694.
[22] P. G. Kevrekidis, *The Discrete Nonlinear Schrödinger Equation: Mathematical Analysis, Numerical Computations and Physical Perspectives*, Vol. 232, Springer Science & Business Media, New York, 2009.
[23] H. Kim, P. Qin, Y. Song, H. Yang, J. Shin, C. Kim, K. Jung, C. Wang, and J. Kim, *Sub-20-attosecond timing jitter mode-locked fiber lasers*, IEEE J. Sel. Top. Quantum Electron, 20 (2014), pp. 260–267.
[24] J. N. Kutz, *Mode-locked soliton lasers*, SIAM Rev., 48 (2006), pp. 629–678.
[25] J. Lu and J. Marzuola, *Strang splitting methods for a quasilinear Schrödinger equation: Convergence, instability, and dynamics*, Commun. Math. Sci., 13 (2015), pp. 1051–1074.
[26] C. Lubich, *On splitting methods for Schrödinger-Poisson and cubic nonlinear Schrödinger equations*, Math. Comput., 77 (2008), pp. 2141–2153.
[27] A. Lunardi, *Analytic Semigroups and Optimal Regularity in Parabolic Problems*, Springer Science & Business Media, New York, 2012.
[28] J. N. Lyness and C. B. Moler, *Numerical differentiation of analytic functions*, SIAM J. Numer. Anal., 4 (1967), pp. 202–210.
[29] J. R. Martins, P. Sturdza, and J. J. Alonso, *The complex-step derivative approximation*, ACM Trans. Math. Software, 29 (2003), pp. 245–262.
[30] C. R. Menyuk and S. Wang, *Spectral methods for determining the stability and noise performance of passively modelocked lasers*, Nanophotonics, 5 (2016), pp. 332–350.
[31] L. F. Mollenauer and R. H. Stolen, *The soliton laser*, Opt. Lett., 9 (1984), pp. 13–15.
[32] R.-M. Mu, V. Grigoryan, C. R. Menyuk, G. Carter, and J. Jacob, *Comparison of theory and experiment for dispersion-managed solitons in a recirculating fiber loop*, IEEE J. Sel. Top. Quantum Electron., 6 (2000), pp. 248–257.
[33] G. Muslu and H. Erbay, *A split-step Fourier method for the complex modified Korteweg-de Vries equation*, Comput. Math. Appl., 45 (2003), pp. 503–514.
[34] R. Paschotta, *Noise of mode-locked lasers (part* I*): Numerical model*, Appl. Phys. B Lasers Opt., 79 (2004), pp. 153–162.
[35] R. Paschotta, *Noise of mode-locked lasers (part* II*): Timing jitter and other fluctuations*, Appl. Phys. B Lasers Opt., 79 (2004), pp. 163–173.
[36] M. Rochette, L. R. Chen, K. Sun, and J. Hernandez-Cordero, *Multiwavelength and tunable self-pulsating fiber cavity based on regenerative SPM spectral broadening and filtering*, IEEE Photonics Tech. Lett., 20 (2008), pp. 1497–1499.
[37] Y. Shen, J. Zweck, S. Wang, and C. R. Menyuk, *Spectra of short pulse solutions of the cubic–quintic complex Ginzburg–Landau equation near zero dispersion*, Stud. Appl. Math., 137 (2016), pp. 238–255.
[38] V. Shinglot and J. Zweck, *The essential spectrum of periodically-stationary pulses in lumped models of short-pulse fiber lasers*, Stud. Appl. Math., 150 (2023), pp. 218–253.
[39] V. Shinglot, J. Zweck, and C. Menyuk, *The continuous spectrum of periodically stationary pulses in a stretched pulse laser*, Opt. Lett., 47 (2022), pp. 1490–1493.
[40] P. Sidorenko, W. Fu, L. G. Wright, M. Olivier, and F. W. Wise, *Self-seeded, multi-megawatt, Mamyshev oscillator*, Opt. Express, 43 (2018), pp. 2672–2675.
[41] O. V. Sinkin, R. Holzlöhner, J. Zweck, and C. R. Menyuk, *Optimization of the split-step Fourier method in modeling optical-fiber communications systems*, J. Lightwave Technol., 21 (2003), pp. 61–68.
[42] K. Tamura, E. P. Ippen, H. A. Haus, and L. E. Nelson, *77-fs pulse generation from a stretched-pulse mode-locked all-fiber ring laser*, Opt. Lett., 18 (1993), pp. 1080–1082.
[43] N. Tarasov, A. M. Perego, D. V. Churkin, K. Staliunas, and S. K. Turitsyn, *Mode-locking via dissipative Faraday instability*, Nat. Commun., 7 (2016), pp. 1–5.
[44] G. Teschl, *Ordinary Differential Equations and Dynamical Systems*, Vol. 140, American Mathematical Society, Providence, RI, 2012.
[45] S. K. Turitsyn, B. G. Bale, and M. P. Fedoruk, *Dispersion-managed solitons in fibre systems and lasers*, Phys. Rep., 521 (2012), pp. 135–203.
[46] H. Uecker, *Hopf bifurcation and time periodic orbits with* pde2path*—Algorithms and applications*, Commun. Comput. Phys., 25 (2019), pp. 812–852.
[47] S. Wang, A. Docherty, B. S. Marks, and C. R. Menyuk, *Comparison of numerical methods for modeling laser mode locking with saturable gain*, J. Opt. Soc. Am. B, 30 (2013), pp. 3064–3074.

[48] S. Wang, A. Docherty, B. S. Marks, and C. R. Menyuk, *Boundary tracking algorithms for determining the stability of mode-locked pulses*, J. Opt. Soc. Am. B, 31 (2014), pp. 2914–2930.
[49] S. Wang, B. S. Marks, and C. R. Menyuk, *Comparison of models of fast saturable absorption in passively modelocked lasers*, Opt. Express, 24 (2016), pp. 20228–20244.
[50] J. Weideman and B. Herbst, *Split-step methods for the solution of the nonlinear schrödinger equation*, SIAM J. Numer. Anal., 23 (1986), pp. 485–507.
[51] S. Wright and J. Nocedal, *Numerical Optimization*, Springer Science & BusinessMedia, New York, 2006.
[52] J. Yang, *Nonlinear Waves in Integrable and Nonintegrable Systems*, SIAM, Philadelphia, 2010.
[53] J. Zweck, Y. Latushkin, J. Marzuola, and C. Jones, *The essential spectrum of periodically stationary solutions of the complex Ginzburg-Landau equation*, J. Evol. Equ., 21 (2021), pp. 3313–3329.